Glaciomarine sediment deposition in the continental slope and rise of the central Ross Sea since the Last Glacial Maximum

Sangbeom Ha[1], Ester Colizza[2], Fiorenza Torricella[3], Leonardo Langone[4], Federico Giglio[4], Gerhard Kuhn[5], Patrizia Macrì[6], Boo-Keun Khim[1*]

[1]Department of Oceanography, Pusan National University, Busan, Korea, [2]Department of Mathematics and Geosciences, University of Trieste, Trieste, Italy, [3]Department of Earth Sciences, University of Pisa, Pisa, Italy, [4]National Research Council-Institute of Polar Sciences, Bologna, Italy, [5]Alfred-Wegener-Institute Helmholtz-Zentrum für Polar- und Meeresforschung (AWI), Bremerhaven, Germany, [6]Istituto Nazionale di Geofisica e Vulcanologia, Rome, Italy

Submitted to Quaternary Science Reviews

*corresponding author: bkkhim@pusan.ac.kr

Abstract

The continental margin of the Ross Sea has been sensitive to the advance and retreat of Ross Ice Sheet (RIS) between the interglacial and glacial periods. This study examines changes in the glaciomarine sedimentation in the continental slope and rise on the eastern side of the Hillary Canyon in the central Ross Sea, using three gravity cores collected with respect to increasing water depth. Based on analytical results and AMS ^{14}C ages of bulk sediments, sediment lithology was divided into units A, B1, and B2, representing interglacial, deglacial, and glacial periods, respectively. The sedimentation rate decreased with increasing water depth, with the glacial sedimentation rate (unit B2) being higher than the interglacial one (unit A). Biological productivity proxies were significantly higher in glacial unit B2 than in the interglacial unit A, with transitional values in the deglacial unit B1. Biological productivity was generally reduced in the Antarctic continental margin during the glacial period because of extensive sea ice coverage. Higher biogenic contents in unit B2 are attributed primarily to the increased transport of eroded and reworked shelf sediments containing more biogenic components to the continental slope and rise beneath the advanced RIS during the glacial period. Thus, glacial sedimentation in the continental slope and rise of the central Ross Sea has been governed by the activity of RIS, which generated melt-water plumes and debris flows at the front of the grounding line, although the continental rise might have experienced seasonally open conditions and lateral effects due to the bottom current.

Key words: sediment core, ice sheet, sea ice, paleoproductivity, continental margin, Ross Sea

1. Introduction

Approximately 98% of Antarctica is covered with ice, which plays an important role in the global water cycle and climate change (Pattyn et al., 2018). If the entire Antarctic ice melts, the global sea level would rise as high as ~60 m above the present-day level, which is equivalent to almost half of the falling range during the last glacial period (DeConto and Pollard, 2016). The Antarctic Ice Sheet (AIS) is geographically divided into the West Antarctic Ice Sheet (WAIS) and the East Antarctic Ice Sheet (EAIS) by the Transantarctic Mountains. The marine-based WAIS grounds largely below sea level and flows rapidly relative to the EAIS (Anderson et al., 2002). Hence, the WAIS responds more sensitively to the changes in seawater temperature and sea level (DeConto and Pollard, 2016). The AIS plays an important role in controlling global climate change such that variations in the extent of the AIS affected surface albedo, global sea level, ocean circulation, and production of bottom water (e.g., Ogura and Abe-Ouchi, 2001; Mackensen, 2004; Ritz et al., 2015).

The WAIS discharges ice into the central and eastern sectors of the Ross Sea, while the EAIS supplies ice to its western sector (Rignot et al., 2008). The Ross Ice Sheet (RIS) has extensively developed mainly from the portions of both with a comparatively higher contribution from the WAIS than the EAIS. The RIS advanced to the shelf edge in the eastern Ross Sea during the Last Glacial Maximum (LGM) (Fig. 1; Anderson et al., 2019). Contrastingly, the RIS did not reach the shelf edge in the central and western Ross Sea and advanced just to the Mawson Bank, Pennell Bank, the southern part of the JOIDES Basin, and the Pennell Trough during the LGM (Fig. 1; Howat and Domack, 2003). The advance and retreat of the RIS significantly influenced the depositional processes and environments in the Ross Sea (Anderson et al., 1984, 2014, 2019; Domack et al., 1999; Prothro et al., 2018).

Unique sedimentary successions associated with activities of the RIS have been well

established on the continental shelf of the Ross Sea. Anderson et al. (2014) reported that diamicton was extensively deposited in the subglacial or glacial-marine setting of the continental shelf during the LGM. Diamicton or subglacial till was also found to have been widely deposited under the grounded ice sheet during the LGM (Prothro et al., 2018; Smith et al., 2019). At this time, frequent debris flow and turbidity current from the front of the grounding line supplied a large quantity of sediments toward the deep basin (Barker et al., 1999). During the period of glacier retreat (i.e., transition time or deglaciation), the ice shelf and the distance from the grounding line controlled the sedimentary processes in the continental shelf (Bart et al., 2017; Prothro et al 2018). The supply of ice-rafted debris (IRD) increased and the lamination of sandy silt was clearly formed as a result of seasonal melt-water outflow from the front of the grounding line during this period (e.g., Smith et al., 2019). During Holocene, warm climate and seasonally open marine conditions allow high primary productivity of diatoms in the surface water, which further leads to more deposition of biogenic sediments (i.e., siliceous mud and ooze) on the western side of the continental shelf, while the Holocene muds on its eastern side contain scarce and reworked diatoms (Langone et al, 1998; Domack et al., 1999; Melis and Salvi, 2009; Anderson et al., 2014; McGlannan et al., 2017; Prothro et al., 2020).

Glaciomarine sedimentation on the continental slope and rise around Antarctica is also influenced by the growth of the AIS (Pudsey, 2000; Caburlotto et al., 2010; Kim et al., 2020; Hillenbrand et al., 2021). During the glacial period, the AIS advanced beyond the continental shelf toward the shelf edge on most of the Antarctic continental margins (e.g., the Ross Sea, the Weddell Sea, and around the Antarctic Peninsula), causing the eroded and unsorted sediments of the continental shelf to be transported toward the upper continental slope by melt-water (Escutia et al., 1997). In addition, the turbidity current also transported the eroded

and reworked hemipelagic sediments of the continental shelf farther into the lower continental slope and rise (Kuvaas and Leitchenkov, 1992; Escutia et al., 1997). Bottom currents formed contourite deposits on the Antarctic continental margin under high sedimentation rates and non-bioturbation during the glacial period (Pudsey 1992; Gilbert et al., 1998; Lucchi and Rebesco, 2007). Such depositional processes during the glacial period led to increased sedimentation rate in the continental slope and rise (Pudsey, 2000); however, evidence for the eroded and reworked shelf sediments has not been reported yet.

Most of the previous studies on the continental slope and rise of the Ross Sea were carried out in its western part (Tolotti et al., 2013; Kim et al., 2020; Torricella et al., 2021). During the glacial period (especially at LGM), more eroded sediments were laterally transported from the continental shelf to the continental slope to the western side of the Iselin Bank in the central Ross Sea (e.g. Kim et al., 2020; Torricella et al., 2021). In contrast, sedimentation and flux of biogenic particles increased on the western side of the Iselin Bank at the beginning of the interglacial period (Ceccaroni et al., 1998). Compared to the western part, few studies have been conducted on the eastern part of the Iselin Bank. In the continental slope to the eastern side of the Iselin Bank, the physical properties (i.e., magnetic susceptibility, bulk density, and P-wave velocity) of sediments indicated that sedimentation patterns were different between the glacial and interglacial periods (Bonaccorsi et al., 2000). For example, structureless or stratified diamicton occurred mainly during the glacial period, while laminated sediments affected by biogenic productivity were commonly deposited during the interglacial period. However, because the studied cores were collected from the channel system, the sedimentary records were incomplete and discontinuous. Furthermore, the geochemical and isotope signatures of continental slope and rise sediments on the eastern part of the Iselin Bank have not yet been studied.

In this study, we investigated three sediment cores collected across the continental slope and rise on the east of the Hillary Canyon in the central Ross Sea (Fig. 1). We have used multi-proxy data, to understand the glaciomarine depositional processes related to the RIS, emphasizing the enhanced re-sedimentation of shelf sediments in the continental slope and rise on the east of the Hillary Canyon in response to the advance of the RIS during glacial periods.

2. Study Area

The Ross Sea is characterized by steep shelf edge, many north-northeast trending basins, troughs and banks (the Drygalski, JOIDES, and Glomar-Challenger Basins, Pennell Trough, and the Crary, Iselin, Mawson, and Pennell Banks), and landward deepening of the continental shelf (Fig. 1). The banks are generally shallower than 500 m. The continental shelf of the Ross Sea is geographically divided into the eastern and western sectors at 180°. The eastern continental shelf consists of broad basins and low-relief banks, while the western continental shelf is characterized by many narrow basins and high banks (Gales et al., 2021). The topography of the inner continental shelf resulted from the repeated advance and retreat of the RIS, where the past ice streams might have flowed toward the deep basin through many deep troughs (Livingstone et al., 2012). These ice streams advanced to the shelf edge, forming many submarine canyons on the continental slope that supplied more sediments to the continental slope and rise. The continental slope of the Ross Sea is also divided into eastern and western parts by the Iselin Bank (Fig. 1). The eastern continental slope is gentle with numerous submarine canyons, whereas the western continental slope is steep with fewer submarine canyons (Gales et al., 2021).

The water masses in the Ross Sea include the Antarctic Surface Water (AASW),

Circumpolar Deep Water (CDW), Antarctic Bottom Water (AABW), and the dense shelf waters including Ice Shelf Water (ISW) and High Salinity Shelf Water (HSSW) (e.g., Castagno et al 2019). The CDW, characterized by higher temperature (>1.5°C) and salinity (>34.60‰), flows along the Ross Gyre and enters into the Ross Sea by the Antarctic Slope Current (ASC), which flows westward along the continental slope following the Antarctic Slope Front (Fig. 1). Some of the CDW flows across the ASC into the continental shelf and is mixed with the AASW which is characterized by low temperature (<-1.85°C) and low salinity (<34.50‰). The dense shelf waters (ISW and HSSW) flows in a cyclonic direction on the continental shelf and connects the grounding line of the Ross Ice Shelf with the continental slope through the troughs on the continental shelf. The HSSW exported from the continental shelf at the northwestern corner of the Ross Sea mixes with CDW as it descends the continental slope, producing the AABW which flows out to the abyssal Australian-Antarctic Basin.

The study area includes the continental slope and rise on the eastern side of the Hillary Canyon in the central Ross Sea (Fig. 1). The Hillary Canyon has developed on the continental slope and rise, with many gullies on the upper continental slope (Gales et al., 2021). These gullies are affected by the AABW and CDW under seasonal open marine conditions (Arrigo and van Dijken, 2004; Smith et al., 2014). The ASC on the continental slope carries the CDW, which intrudes the continental shelf (Smith et al., 2014). During the glacial period, the intrusion of CDW to the continental shelf was blocked by the advanced ice sheet, but could affect the continental slope at the eastern side of Hillary Canyon because the ASC moved northward (Gales et al., 2021). Compared to the continental shelf, primary productivity in the continental slope and rise is lower, because the seasonal sea ice remains longer in the eastern part of the Ross Sea (Arrigo and van Dijken, 2004; Smith et al., 2014).

3. Materials and Methods

Three gravity cores (GC1, GC2, and GC3) and three box cores (BC1, BC2, and BC3) were obtained at three stations (RS14-C1, C2, and C3) across the continental slope and rise on the east of the Hillary Canyon (central Ross Sea) during the XXIX Italian PNRA (National Antarctic Research Program) Expedition (PNRA–ENEA/UTA, 2014) under the Italian project ROSSLOPE Ⅱ (Fig. 1, Table 1). Box cores were used to check the loss of the gravity cores and the core-top age, whereas gravity cores were used to reconstruct the changes in glaciomarine sedimentation. The obtained cores were split, visually described, and photographed at the University of Trieste (Italy). Sediment samples for the experimental analyses were taken at 4 cm intervals for all the box cores and the upper parts (core-top to 34 cm in GC2, and to 38 cm in GC3 and GC1) of the gravity cores and at 8 cm intervals for the lower parts of the gravity cores (rest of the core sections to core-bottom). All analytical data are summarized in Supplementary Data File.

Magnetic susceptibility (MS) measurements were conducted using a Bartington magnetic susceptibility meter equipped with probe MS2C at 1 cm interval at the paleomagnetic laboratory of the Istituto Nazionale di Geofisica e Vulcanologia (Italy). Before grain size analysis, the organic matter was removed using hydrogen peroxide and the remaining sediments were sieved using a 2-mm sieve net. Biogenic silica and carbonate were not eliminated. Sediment particle sizes <2 mm were determined using a Malvern Mastersizer Hydro2000S diffraction laser unit at the University of Trieste (Italy). Sand, silt, and clay fractions were classified according to the scheme of Friedman and Sanders (1978). Particles >2 mm were counted. To identify the preliminary mineral composition of IRDs at 38 cm (i.e., the highest amount of IRDs) of GC3, several IRDs were powdered for the X-ray

186 diffractometer (XRD; Siemens/Brucker D5005) operation and selected grains were
187 photographed and examined by scanning electron microscope-energy dispersive spectrometry
188 (SEM-EDS) analyzer (JSM-6380LV) at Gyeongsang National University (Korea).

189 Sediment samples were freeze-dried and powdered for geochemical analyses conducted
190 at Pusan National University (Korea). Total carbon (TC) and total nitrogen (TN) contents
191 were measured using a CHN elemental analyzer (Flash 2000 Model). The analytical error of
192 the instrument is ±0.1%. Total inorganic carbon (TIC) was measured using a UIC CO_2
193 Coulometer (CM5014 Model). The analytical error of the instrument is ±0.1%. Calcium
194 carbonate ($CaCO_3$) content was calculated by multiplying the TIC content by 8.333. Total
195 organic carbon (TOC) was calculated by subtracting TIC from TC. The C/N ratio was
196 calculated by dividing the TOC by TN. Biogenic silica content was analyzed using the wet
197 alkaline extraction method (DeMaster, 1981). The analytical precision as a relative standard
198 deviation (±1σ) is 1%. Biogenic opal content was calculated by multiplying the biogenic
199 silica by 2.4 (Mortlock and Froelich, 1989).

200 Carbon isotopic composition ($\delta^{13}C$) of carbonate-free sediments and nitrogen isotopic
201 composition ($\delta^{15}N$) of bulk sediments were measured using a Finnigan Delta Plus XP mass
202 spectrometer directly coupled with a Thermo Fisher Scientific FLASH 2000 isotope ratio
203 mass spectrometer elemental analyzer at Istituto di Scienze Polari-Consiglio Nazionale delle
204 Ricerche (ISP-CNR, Italy). All isotopic compositions were expressed in the conventional δ
205 notation and reported as parts per thousand (‰):

206 $$\delta^{13}C = [(^{13}C/^{12}C)_{sample} / (^{13}C/^{12}C)_{VPDB} - 1] \times 10^3$$

207 $$\delta^{15}N = [(^{15}N/^{14}N)_{sample} / (^{15}N/^{14}N)_{air} - 1] \times 10^3$$

208 As determined from the routine repeat measurements of the reference sample IAEA-CH7
209 (polyethylene, -32.15‰ vs. Vienna Peedee Belemnite, VPDB), uncertainties were lower than

±0.5‰. The internal standard for $\delta^{15}N$ measurements was IAEA-N-1 (ammonium sulfate, +0.4‰ vs. air). Error for repeat analyses of the standard was ±0.2%.

The ^{14}C dating using the accelerator mass spectrometry (AMS) was carried out for the core-top of the box cores (BC1, BC2, and BC3) and four horizons of each gravity core (GC1, GC2, and GC3) (Table 2). Due to the scarcity of foraminifera in the studied samples, the AMS ^{14}C activity of sediments was measured on acid-insoluble organic matter (AIOM) of the bulk sediments at the Poznàn Radiocarbon Laboratory of Adam Mickiewicz University (Poland) and with MICADAS (Wacker et al., 2013) at the AWI (Mollenhauer et al., 2021) (Germany). The results of AMS ^{14}C using the AIOM fraction of bulk sediments are often compromised by contamination from older carbon derived from glacial erosion and/or from the reworking of unconsolidated sediments (e.g. Andrews et al., 1999; Pudsey et al., 2006; Mezgec et al., 2017; Tesi et al., 2020). The AIOM ages of the core-top (0–1 cm) of BC01, BC02, and BC03 were used to correct the respective ages of the deeper parts for each gravity core. These ages embed the regional marine reservoir effect (MRE) and the local dead carbon contamination offset (LCO). Before calibrating the ^{14}C ages, the LCO obtained for the study area was subtracted from the AIOM ^{14}C box core ages (LCO-corrected ages), assuming that both MRE and LCO did not change during the Holocene and glacial periods (see Hall et al., 2010; Hillenbrand et al., 2010). The LCO-corrected AMS ^{14}C ages were converted into calibrated ages using the CALIB REV 7.1 program (Stuiver et al., 2018) at 95% confidence. Assuming the regional marine offset (ΔR) to be 0.79±0.12 ka from the global MRE (Hall et al., 2010), the MARINE 13 calibration curve (Reimer et al., 2013) was used. The new calibration curve (MARINE 20) was not used because it is not suitable for the calibration of Antarctic sediments (Heaton et al., 2020). Uncorrected and calibrated AMS ^{14}C ages are summarized in Table 2. All ages reported in this study are calibrated ages (cal. yr BP), unless

otherwise specified. The calibrated ^{14}C ages of the three gravity cores show no age reversal except for one age in GC1, resulting in the reasonable establishment of sequential stratigraphic order corresponding to the lithologic units.

4. Results

4.1. Core-top comparison

A fair amount of the top of gravity corer was lost during the coring process. Geochemical properties of the box core and the upper part of the gravity core were compared to identify the core-top loss. Figure 2 shows a comparison of TOC, TN, and $CaCO_3$ contents between the two cores. Both variation patterns coincided with each other. The difference at the core-top is <0.06% of TOC, <0.01% of TN, and <0.2% of $CaCO_3$ at sites C1 and C2. At site C3, the difference was 0.3% of TOC, 0.02% of TN, and 2% of $CaCO_3$, respectively. Most of these differences were within the analytical error range. Based on this comparison, it was estimated that approximately a few centimeters of sediments were lost from the core-top of gravity cores. Such negligible losses suggested that the core-top of the gravity cores was well preserved and had recorded the latest Holocene period, despite the relatively old ^{14}C ages (Table 2).

4.2 Lithologic units (A, B1, and B2)

Based on the sediment color, core description, and analytical properties, the lithology of the three gravity cores was divided into two main units (A and B), and lithologic unit B was further divided into two subunits (B1 and B2) (Fig. 3). Lithologic unit A is characterized by brownish hemipelagic silty mud, enriched IRDs (~14 #/cm^3 in GC3 and ~5 #/cm^3 in GC2 and GC1), and high sand fraction (from 9% in GC1 to 32% in GC3) with more fluctuation of MS

intensity (Fig. 3). The number of IRDs and sand content of unit A decreased away from the shelf margin toward the continental rise (Fig. 3). The MS intensity appears to depend on the number of IRDs and the sand content.

Grayish sediment color is common in unit B, but the lithologic features are different between units B1 and B2. Unit B1 consists of sandy mud, whereas unit B2 is composed of hemipelagic silty mud with sparse/scattered IRDs (Fig. 3). Unit B1 shows an upward increase in the IRDs and sand fraction with the MS peak at the top of it. In contrast, unit B2 contained very rare to sparse IRDs (2~4 #/cm^3) and low sand fractions (~13%), and the number of IRDs was higher in the lower part than in the upper part.

Characteristic mineral and elemental compositions were obtained from representative IRDs from GC3 (Figs. 4 and 5). The IRDs mainly consisted of quartz and mica with accessory chlorite, kaolinite, plagioclase, and muscovite (Fig. 4). A distinct peak of hornblende was observed at the horizon of 38 cm depth, which also contained abundant mica. According to SEM-EDS analysis (Figs. 5 and S1), IRD grains are enriched in Si and Al, which confirms that the dominant mineral composition is aluminosilicate. Another interesting feature is the detection of the Ca peak in some grains, which may be attributed to the carbonate minerals. However, a distinct calcite peak was not detected in XRD studies, presumably due to its very low amount. Nevertheless, the high $CaCO_3$ content (~8%) at this horizon of GC3 might be due to the occurrence of detrital grains.

The bulk and isotope geochemistry of unit A generally revealed low biogenic opal (3.6~5.4%), TOC (0.16~0.22%), $\delta^{13}C$ (-25.2 to -24.7‰), $CaCO_3$ (0.2~0.3%), and C/N ratio (6.7~9.1), with slightly high TN (~0.03% in GC3 and GC2) and $\delta^{15}N$ (4.6 to 4.9‰) (Fig. 6). Units B1 and B2 can also be distinguished by their bulk and isotope geochemistry. Unit B2 is characterized by a lower TN (~0.02%) and $\delta^{15}N$ (3.8 to 4.9‰) and higher biogenic opal

(~11.0%), TOC (0.30~0.36%), $\delta^{13}C$ (-24.8 to -24.6‰), $CaCO_3$ (~1.7% in GC3 and GC2 and ~0.3% in GC1). Conversely, unit B1 was characterized by transitional values between units B2 and A, i.e., biogenic opal (11.1~5.0%), TOC (0.33~0.19%), $\delta^{13}C$ (-24.7 to -24.8‰), $CaCO_3$ (1.2~0.2%), TN (0.02~0.03%), and $\delta^{15}N$ (4.5 to 4.7‰) (Fig. 6).

4.3 Lithologic units of the gravity cores

The three gravity cores (GC3, GC2, and GC2) have the same lithologic succession (units A, B1, and B2) (Fig. 3). GC3 consists of the three units (A, B1, and B2). In addition to the three units, GC2 contains an additional very thin (10 cm) unit A at the bottom of core. Contrastingly, the lithologic sequence (A, B1, and B2) was repeated 3 times in GC1.

Downcore geochemical and isotopic profiles of the three gravity cores confirmed the configuration and succession of lithologic units in them (Fig. 6). Despite different contents, variation patterns of the geochemical and isotopic results for each lithologic unit were similar among the three cores. Unit A is characterized by the low biogenic opal, TOC, $\delta^{13}C$, C/N ratio, $CaCO_3$, and high TN and $\delta^{15}N$. Biogenic opal content decreased slightly with increasing water depth (from GC3 to GC1), whereas the TOC content, $\delta^{13}C$ value, and $\delta^{15}N$ value increased slightly with increasing water depth. Unit B1 marks the transition between units (A and B2), and is represented by a distinct decrease in biogenic opal content, TOC content, $\delta^{13}C$ value, TN content, C/N ratio, and $CaCO_3$ content and slight increase of $\delta^{15}N$ value. However, the geochemical properties of GC1 in the continental rise show slightly different variations from the other two cores in the continental slope. TOC and $CaCO_3$ contents and $\delta^{15}N$ and $\delta^{13}C$ values were similar in unit A for all cores. In contrast, TN content (*ca*. 0.02%) and biogenic opal content (*ca*. 9%) in unit A of GC1 were lower and higher, respectively, than those of the other two cores (*ca*. 0.04% and *ca*. 5%, respectively). The geochemical

properties of unit B1 of GC3 and GC2 are transitional between units B2 and A, but this transition was not clear in GC1. In addition, TOC content of unit B2 in GC1 was slightly higher (*ca*. 0.5%) than that of the other cores (*ca*. 0.3%). Particularly, biogenic opal content of GC1 was similar in units A and B2 (~9%). $\delta^{15}N$ and $\delta^{13}C$ values of GC1 also fluctuated significantly within unit B2, being slightly lower and higher, respectively, than those of the other two cores. A much lower $CaCO_3$ content (0.4%~1.0%) was observed in unit B2 of GC1, compared to the other cores (3.0%).

5. Discussion

5.1. Sediment deposition in the continental slope and rise of the central Ross Sea

The core-top ages for GC3, GC2, and GC1 are 1.5 ka, 5.7 ka, and 2.5 ka, respectively (Table 2). Such old ages in core-tops are generally observed in the Antarctic Ocean (e.g. Licht et al., 1996; Hall et al., 2010). Based on these AMS ^{14}C ages, the uppermost part of the three gravity cores should represent the Holocene accumulation, which makes lithologic unit A the interglacial sediment. Consequently, lithologic unit B, which underlies unit A, represents the glacial and deglacial (B1 and B2, respectively) sediments, based on the depositional order (Fig. 6). The old AMS ^{14}C ages in unit B1 are mainly due to the redeposition of old sediments on continental slope and rise by turbidity current or mass accumulation processes during the glacial period (e.g., Pudsey, 2000). Although GC3 consists of units A and B, it may not have recorded a complete interglacial-glacial cycle, compared to GC2 and GC1 that show repetition of lithologic successions.

Sedimentation rate of unit A prominently decreases with increasing water depth (6.3 cm/kyr at GC3, 2.0 cm/kyr at GC2, and 1.2 cm/kyr at GC1). In general, the supply of terrigenous sediments decreases further from the Antarctic coastal regions (Grobe and

Mackensen, 1992; Domack et al., 1999; Pudsey., 2000; Prothro et al., 2018). Thus, the lowering of the Holocene sedimentation rate with increasing water depth is typical because the continental shelf of the Ross Sea lies at a further distance from the continental slope and rise. Similar to unit A, the sedimentation rate of unit B (~9.0 cm/kyr by extrapolation at GC3, 2.6 cm/kyr at GC2, and 1.7 cm/kyr at GC1) also decreases with increasing water depth. However, it should be noted that the sedimentation rate is distinctly higher in unit B than in unit A, which indicates a greater sediment supply to the continental slope and rise during the glacial period than during the interglacial period. Increased sedimentation rates during the glacial period have been reported in the continental slope of the Antarctic Peninsula and Wilkes Land (Pudsey and Camerlenghi, 1998; Pudsey, 2000; Tooze et al., 2020). Similar to the continental shelf, sediment deposition on the continental slope and rise around Antarctica has changed in response to the activity of the AIS between the glacial and interglacial periods (e.g., Anderson et al., 2014). During the glacial period, glacial tills were deposited on the edge of the continental shelf and the upper continental slope, and then transferred to the lower continental slope and continental rise by the turbidity currents (Larter and Barker, 1989; Pudsey, 2000). For example, Grobe and Mackensen (1992) highlighted the importance of the melt-water underneath the ice sheet and gravity flow from the shelf edge or upper continental slope in transporting the sediments to the lower continental slope and continental rise in the Weddell Sea at the LGM. Thus, glacial activity caused increased sedimentation in the continental slope and rise of the central Ross Sea during the glacial period, although there might have been some inputs from the bottom current as well.

The sediments of unit A commonly contained IRDs (Fig. 3). The brownish sediments in the Antarctic Ocean generally represent seasonal sea ice conditions during the warm interglacial period (Grobe and Mackensen 1992; Pudsey and Camerlenghi, 1998; Pudsey,

354 2000). The MS intensity is normally high for both diamicton and glacial till in the continental
355 shelf during the glacial period, otherwise, due to the IRD-enriched coarse-grained sediments
356 deposited during the interglacial period (Licht et al., 1999; Salvi et al., 2006; Smith et al.,
357 2019). Grobe and Mackensen (1992) reported that interglacial IRDs increased in the eastern
358 Weddell Sea and Ó Cofaigh et al. (2001) reported that IRDs peaked toward the end of the
359 glacial period with an increase in seawater temperature and sea level in the Bellingshausen
360 Sea. The MS intensity of unit A in the studied three cores was influenced by the number of
361 IRDs and sand fraction (Fig. 3). Many IRDs in unit A could reflect that sediment deposition
362 was influenced by an increase of calving events during the warm period. The IRDs originated
363 from the continent and were transported by icebergs from the calving line of the RIS to the
364 continental shelf. Ha et al. (2018) reported the clay mineral composition of fine-grained
365 sediments of GC2. Unit A of GC2 was characterized by lower illite and higher smectite and
366 kaolinite. This indicates that the supply of illite by melt-water from the Antarctic continent
367 decreased whereas the supply of smectite and kaolinite increased due to the westward
368 flowing ASC from the Marie Byrd Land to the study area during the Holocene. Thus, the
369 supply of unit A sediments transported by icebergs and currents from the inner continental
370 shelf increased causing increased sedimentation in the continental slope and rise on the east
371 of the Hillary Canyon, whereas the supply by melt-water or debris flow under the ice sheet or
372 ice shelf decreased due to the retreat of the RIS on the continental shelf.

373 Unit B1 of all three cores was characterized by the increasing IRDs and fluctuations of
374 MS intensity with the sand fraction, suggesting that unit B1 could represent the transitional
375 phase between the glacial and interglacial periods. McKay et al. (2008) reported that sandy
376 sediments in the Ross Sea were supplied from the Transantarctic Mountains, including the
377 McMurdo volcanic group, through the advance and retreat of the RIS. The mineral

composition of IRDs (at 38 cm in unit B1 of GC3) is mainly aluminosilicates with significant hornblende and mica (Figs. 4 and 5). The hornblende might have been supplied from the igneous and high-grade metamorphic rocks in the Transantarctic Mountains (Licht et al., 2005). The grayish sediments of unit B2 are characterized by sparse IRDs and slight fluctuations in MS intensity (Fig. 3). The grayish sediments in the Antarctic Ocean were commonly deposited during the glacial period (e.g. Grobe and Mackensen, 1992; Pudsey and Camerlenghi, 1998; Pudsey, 2000). In addition, fewer IRDs were supplied during the glacial period because of lower iceberg formation (Smith et al., 2019). The fine-grained sediments of unit B2 of GC2 are characterized by more illite and less smectite and kaolinite (Ha et al., 2018). This indicates that during the glacial period, fine-grained sediments containing more illite may have been transported from the Antarctic continent toward the continental slope and rise on the east of the Hillary Canyon by the melt-water under the part of the RIS that advanced to the shelf edge. It also indicates that unit B contains continental shelf sediments reworked and transported by melt-water or debris flow beneath the advanced RIS.

5.2. Change of geochemical and isotopic properties among the lithologic units

Biogenic productivity in the surface water around the continental margin of the Ross Sea mainly depends on the degree of seasonal sea ice coverage and nutrient availability (Smith et al., 2014). During winter, the surface water is covered with sea ice; thus, very low amount of biogenic flux is supplied only from the polynya areas which have formed in front of the Ross Ice Shelf due to katabatic winds (Langone et al., 2000). During the spring to summer, the sea ice begins to disappear from the western part of the continental shelf, and phytoplankton (*Phaeocystis antarctica*) starts to bloom in the surface water (Arrigo et al., 2000). After the sea ice disappears completely, the second bloom by diatom (*Fragilariopsis*

curta) at the front of the Ross Ice Shelf allows the sedimentation of siliceous ooze on the continental shelf (Arrigo et al., 2000). The appearance of *F. curta* has been reported in the Glomar-Challenger Basin of the central Ross Sea and the outer continental shelf of the Wales Deep Basin in the eastern Ross Sea (Tolotti et al., 2013; McGlannan et al., 2017).

The surface sediments in the continental shelf of the Ross Sea consist of siliceous ooze and residual glaciomarine sediments (Langone et al., 1998; Porthro et al., 2018). These present-day siliceous mud and ooze are associated with the seasonal sea ice and polynya of the surface water (Arrigo et al., 2000). Conversely, residual glaciomarine sediments at the top of the banks were deposited mostly by reworking of surface sediments by the bottom current (Anderson et al., 1984). TOC content of the surface sediments in the present-day continental shelf of the Ross Sea lies between ~0.2 and ~2.0% (Ledford-Hoffman et al., 1986; Frignani et al., 1992; Langone et al., 1998; McKay et al., 2008; Tolotti et al., 2013). TN content also increased up to ~0.1% and the biogenic opal content varied from ~10% to >30%. TOC content increases with an increase of biogenic opal, but biogenic opal content is higher in the western part of the Ross Sea than in the northern and central parts (Langone 1998).

Unit A is interpreted as the interglacial sediments and shows a low degree of biogenic productivity, denoted by TOC, TN, and biogenic opal, in the continental slope and rise of the central Ross Sea, compared with the surface sediments in the continental shelf. Such low biogenic productivity can be attributed to less phytoplankton bloom during the long duration of sea ice coverage on the surface water leading to low nutrient availability (Arrigo et al., 2000; Smith et al., 2014). The surface water conditions of the Antarctic continental margin have changed over time between permanent multi-year ice and seasonal open marine conditions, depending on the sea level rise and seawater temperature increase (e.g. Grobe and Mackensen, 1992; Pudsey, 2000; Kim et al., 2020). After the LGM, the biogenic properties

increased with the development of seasonal open marine conditions on the continental shelf of the Ross Sea (e.g. Cunningham et al., 1999; Domack et al., 1999; Salvi et al., 2006) and continental slope of the Antarctic Peninsula and Weddell Sea (Grobe and Mackensen, 1992; Pudsey, 2000). The distinct increase of biogenic properties within unit A in three cores indicates the development of seasonal open marine conditions with an increase of primary productivity in the surface water during the late Holocene.

The geochemical properties of unit B1 are transitional from the glacial unit B2 to the interglacial unit A (Fig. 6). Notably, TOC, TN, and biogenic opal contents of unit B were higher than those of unit A, which indicates enhanced biogenic productivity of unit B. This implies that glacial productivity was higher than the interglacial productivity in the continental slope and rise of the central Ross Sea. However, it contradicts the previous results that showed biogenic productivity in the Ross Sea to be higher during the interglacial period than during the glacial period (Brambati et al., 1997; Cunnuningham and Leventer, 1998; Salvi et al., 2006; Kim et al., 2020). During the glacial period, biogenic production decreased significantly in the continental shelf of the Ross Sea, because of the advanced RIS and permanent sea ice. Because of the limited light due to the permanent or multi-year sea ice, primary production in the continental slope and rise is generally reduced during glacial periods (Grobe and Mackensen, 1992). Thus, the higher geochemical contents of unit B, representing a high degree of productivity, were probably due to alternative processes.

As explained above, primary productivity in the continental margin of the Ross Sea was lower during the glacial periods due to the advanced RIS and extensive sea ice cover (e.g., Ceccaroni et al., 1998). Nevertheless, TOC, TN, and biogenic opal contents of unit B2 were almost similar to those of the present-day sediments on the continental shelf. During the glacial period, continental shelf sediments were covered with the advanced RIS. Increased

sediment supply to the continental slope and rise due to glacier activity and melt-water of glacial plumes is evidenced by the higher sedimentation rate in unit B. During the interglacial period, the continental shelf sediments contained more biogenic particles (Ledford-Hoffman et al., 1986; Frignani et al., 1992; Langone et al., 1998; McKay et al., 2008; Tolotti et al., 2013). High biogenic content-bearing shelf sediments were found to be eroded by advanced AIS and transported by melt-water or ice along with other terrigenous materials from the shelf edge to the continental slope and rise (Grobe and Mackensen, 1992; Pudsey, 2000; O'Brien et al., 2020). Thus, the glacier activity and melt-water underneath the ice sheet, which advanced to the shelf edge during the glacial period, led to reworking and transporting the biogenic particle-enriched shelf sediments to the continental slope and rise, resulting in high biogenic contents of unit B2. In addition, the upward decrease of biogenic content from unit B2 to unit B1 could indicate a lower supply of shelf sediments during deglaciation due to the retreat of RIS. Our results conform with Khim et al. (2021) who reported that the deglacial and glacial sediments in the Central Basin of the northwestern Ross Sea are characterized by higher TOC and biogenic opal contents than the Holocene sediments.

Our interpretation is also supported by correlation between the geochemical properties (Fig. 7). In general, TOC and TN contents is linearly correlated with different slopes depending on the marine or terrestrial origin. C/N ratio identifies the origin of organic matter, and a higher C/N ratio represents a greater contribution of terrestrial or regenerated organic matter (Meyers, 1994). The relationship between TOC and TN contents of unit A of the cores is different from that of units B1 and B2, except for GC1 (Fig. 7). During post-depositional oxidation of organic matter within the sediments, organic nitrogen degrades more easily than organic carbon (Kristensen and Blackburn, 1987), resulting in the degraded organic matter being slightly enriched in organic carbon. Compared with unit A, TOC content of units B1

and B2 were enriched relative to TN content, indicating that the presence of degraded organic matters in units B1 and B2.

The positive relationship between TOC content and C/N ratio demonstrates that higher TOC content and C/N ratio of units B2 and B1 are attributed to the input of more terrestrial organic matter and not marine diatom production. However, more supply of terrestrial organic matter to the study area is difficult in the present-day scenario, because it is located further away from the coastal areas. During the glacial period, the advanced RIS might have transported terrestrial organic matter toward the shelf edge, which can be the reason for the prominent terrestrial influence on the continental slope and rise. However, the differential degradation between organic carbon and nitrogen during post-deposition caused an increase in C/N ratio (Kristensen and Blackburn, 1987), resulting in its positive relationship with TOC content. Thus, instead of glacial activity, the strong correlation between high TOC content and C/N ratio of units B1 and B2 can be attributed to the regenerated organic matter of the eroded shelf sediments that preserved the interglacial biogenic components.

Although Site C1 in the continental rise is located farther from the shelf edge than Sites C2 and C3 (Fig. 1), TOC (~0.6%), TN (up to 0.033%), and biogenic opal (up to 30%) contents of unit B2 in GC1 is higher than GC2 (~0.2%, 0.025%, and ~16%, respectively) and GC3 (~0.3%, 0.026%, and ~16%, respectively) (Fig. 6). Because the sedimentation rate of unit B2 decreases with increasing water depth, sediment supply from the shelf edge to Site C1 was reduced. Thus, the high biogenic contents in GC1 as compared to GC2 and GC3 might be due to some other factors. Furthermore, it is noteworthy that the relationship between TOC and TN content was similar between units A and B2 in GC1 (Fig. 7). This implies that the additional seasonal production might have occurred at Site C1 in the surface water of the continental rise during the glacial period. Ice free areas, so called polynyas, are

generally developed by either katabatic winds from the continent or upwelling of relatively warm deep water (Martin, 2001). Grobe and Mackensen (1992) and Smith et al. (2010) suggested the possible formation of glacial polynya in the continental rise of the Weddell Sea during the glacial periods. Pudsey (2000) also reported that diatom production occurred in the polynya which had developed on the continental rise of the Antarctic Peninsula during glacial periods. The warm CDW could not intrude into the continental shelf because of the advanced RIS; thus it melted the ice front during glacial periods (e.g. Gales et al., 2021). The temporary polynya on the continental rise might have formed by upwelling warm water which was blocked by an ice sheet. Thus, higher biogenic contents in unit B2 of GC1, representing the degree of productivity, indicate that permanent sea ice did not cover the entire continental rise in the central Ross Sea during glacial periods.

$CaCO_3$ content of the studied cores was generally low (up to ~0.2%) in unit A, and slightly high (~2% in GC2 and GC3 and ~0.5% in GC1) in unit B (Fig. 6). Such low $CaCO_3$ content of Holocene sediments is common in the Antarctic continental margin. Anderson (1975) reported that the dissolution of $CaCO_3$–bearing phases during the interglacial periods in the Weddell Sea was caused by the increased production of corrosive dense bottom water (i.e., CO_2-rich AABW), which intensified its dissolution on the seafloor. Kim et al. (2020) reported that the continental shelf edge sediments of the Iselin Bank in the central Ross Sea contained low $CaCO_3$ content during interglacial periods, which is partly attributed to the increasing effect of dense shelf water and CO_2-enriched CDW and partly to dilution by fine siliceous detritus. Thus, the slightly high $CaCO_3$ content during glacial periods may also be due to less dissolution on the continental slope and rise in the central Ross Sea, which can be related to a sinking of the calcite compensation depth as a result of a northward shift of the polar front in the Southern Ocean.

522 The $\delta^{13}C$ and $\delta^{15}N$ values of sedimentary organic matter are controlled by diverse
523 factors (summarized in Altabet, 1996). The $\delta^{13}C$ values of organic particles depend mainly on
524 changes in $[CO_2]_{aq}$ and seawater temperature, type of autotrophic species (marine or
525 terrestrial), and/or diagenetic alteration, along with growth rate and species diversity of
526 phytoplankton (Rau et al., 1997). Similarly, the $\delta^{15}N$ values of particulate organic matter are
527 influenced mainly by the dynamics of inorganic nitrogen compounds in surface water
528 (Altabet, 1996), and to a lesser extent, by the trophic structure of the ecosystem (DeNiro and
529 Epstein, 1981). The $\delta^{13}C$ and $\delta^{15}N$ values of the deep sea sediments have been used to trace
530 paleobiogeochemical changes in the surface ocean that can be related to paleoproductivity
531 and atmospheric pCO_2 levels (Francois et al., 1992; Altabet et al., 1995). Despite many
532 complicated factors present in the Antarctic continental margin, $\delta^{13}C$ and $\delta^{15}N$ values of
533 organic matter, assimilated during enhanced production conditions in the warm interglacial
534 period, are generally higher (Rau et al., 1991; Villinski et al., 2000; Robinson and Sigman,
535 2008). It is interesting that unit A is characterized by low $\delta^{13}C$ (-25.2 to -24.7‰) and high
536 $\delta^{15}N$ (4.6 to 4.9‰) values whereas unit B2 is characterized by slightly high $\delta^{13}C$ (-24.8 to -
537 24.6‰) and slightly low $\delta^{15}N$ (3.8 to 4.9‰) values with transitional values in unit B1 (Fig. 6).
538 These isotope results seem unlikely to vary depending on interglacial and glacial conditions.
539 The $\delta^{13}C$ and $\delta^{15}N$ values of unit A are assumed to represent the seasonal production of *in situ*
540 organic particles during the warm interglacial periods. The slightly higher $\delta^{13}C$ values of
541 units B1 (deglacial) and B2 (glacial), as compared to that of unit A, are not a result of
542 enhanced production as the case of biogenic TOC and TN. Such a slight increase in $\delta^{13}C$
543 values of units B1 and B2 may be attributed to the incorporation of regenerated organic
544 matter from the shelf sediments that underwent selective diagenesis and/or a greater
545 contribution of sea ice-originated organic matter. The slightly low $\delta^{15}N$ values of units B1

546 and B2 also support the theory of limited production during cold glacial periods with
547 relatively more contribution of sea ice-originated organic matter (Cozzi and Cantoni, 2011).
548 Although units A and B might be distinguished by $\delta^{13}C$ and $\delta^{15}N$ values with respect to *in situ*
549 surface water productivity, more precise examination and robust interpretation will be
550 required due to the complicated factors responsible for their values in the Antarctic organic
551 particles.
552
553 **5.3. Paleoenvironmental reconstruction in the continental slope and rise of the central**
554 **Ross Sea**
555 Figure 8 depicts the schematic paleoenvironmental model in terms of glaciomarine
556 sedimentation in the continental slope and rise on the east of the Hillary Canyon in the central
557 Ross Sea. The Antarctic environment has been strongly affected by the advance and retreat of
558 ice sheet, which interacted with the developing ice shelf and seasonal sea ice (Anderson et al.,
559 1980; Grobe and Mackensen 1992; Domack et al., 1999; Pudsey 2000). During the glacial
560 period, the grounding line of the advanced RIS was located near the shelf edge on the east of
561 the Pennell Bank and the sea ice coverage extended toward the continental slope and rise
562 (Shipp et al., 1999; Anderson et al., 2002). During this time, the pressure of advanced RIS
563 caused extensive erosion of the continental shelf, resulting in the deposition of diamicton
564 (Anderson et al., 1984; Domack et al., 1999). Unit B2 of the study area could represent the
565 glacial sediments, where the permanent sea ice covered the continental slope and rise on the
566 east of the Hillary Canyon. Thus, the unsorted sediments of unit B2 were mainly supplied
567 from the continental shelf by melt-water or debris flow through erosion of the advanced RIS
568 to the continental slope and rise (Fig. 8a). The amount of sediment transport decreased with
569 increasing distance from the continental shelf, where the sediments were eroded and

570 reworked. Consequently, the sedimentation rate of unit B2 decreased from GC3 to GC1 (Fig.
571 3). Reduced primary productivity (in terms of biogenic content) in the continental slope and
572 rise of the central Ross Sea, compared with the interglacial periods, was observed. Glacial
573 productivity was also very low on the continental slope and rise of the western Ross Sea
574 (Ceccaroni et al., 1998; Kim et al., 2020), Antarctic Peninsula (Pudsey, 2000), and Weddell
575 Sea (Grobe and Mackensen, 1992). Based on TOC and biogenic opal contents, GC1 located
576 in the lower continental rise recorded seasonal sea ice coverage or occurrence of limited
577 polynya, supplying *in situ* biogenic sediments. The low smectite content of unit B2 in GC2
578 indicates that the clockwise surface current in the continental shelf was blocked by the
579 advanced RIS (Ha et al., 2018). In addition, because of the advanced RIS on the eastern
580 continental shelf, the production of corrosive AABW was restricted, resulting in slightly
581 better preservation of $CaCO_3$ in the study area.

582 After the LGM, the RIS began to retreat rapidly on the continental shelf of the eastern
583 Ross Sea (Mosola and Anderson, 2006). During the deglacial period, the depositional process
584 depended on the distance from the grounding line of the retreating ice sheet and ice shelf
585 (Domack et al., 1999; Smith et al., 2019). Grounding zone wedge at the front of the
586 grounding line, fine-grained sediment deposition beneath the ice shelf, and sinking of
587 biogenic particle under the seasonal open marine conditions occurred on the continental shelf
588 of the western Ross Sea (Domack et al., 1999). The permanent sea ice changed into multi-
589 year or seasonal sea ice during this period in the continental slope and rise of the Weddell Sea
590 and Antarctic Peninsula (Grobe and Mackesen 1992; Pudsey, 2000). Similarly, the sea ice in
591 the continental slope and rise of the central Ross Sea, which resulted in a gradual increase of
592 biological production, might be multi-year or seasonal (Fig. 8b). The effect of RIS on the
593 continental slope and rise was significantly reduced, and sediment supply from the

continental shelf by melt-water or debris flow was also diminished. The sediment properties of unit B1 changed gradually from unit B2 (glacial) to unit A (interglacial). An increase in IRDs in unit B1 reflects seawater temperature rise, collapse of retreated ice shelf, and production of icebergs during the deglaciation (Barker et al., 1999; Salvi et al., 2006).

During the Holocene, the environment in the continental margin of the Ross Sea is characterized by seasonal open marine conditions, in which the biological productivity of surface water enhances in spring and summer (Anderson et al., 1984). However, biological productivity mainly occurs in the southern and western parts of the continental shelf in the Ross Sea (Arrigo et al., 2000; Arrigo and van Dijken, 2004). The surface sediments in the Ross Sea are characterized by abundant biogenic particles in deep basins and troughs, remnant sediments winnowed by bottom currents on shallower banks, and IRDs transported by icebergs from the calving line (Anderson et al., 1984). The higher percentage of gravel and sand fraction in unit A is related to the increasing supply of IRDs by icebergs due to the increase in seawater temperature and the sea level rise. The increase in biogenic contents of unit A, represented as surface water productivity, indicates enhanced biological productivity during the Holocene (Fig. 8c). The high smectite content of unit A reflects that the surface current in the continental shelf of the Ross Sea flows clockwise from Victoria Land toward the continental slope (Ha et al., 2018). With the complete retreat of the RIS, nutrient-enriched CDW intruded the inner continental shelf and corrosive AABW was actively produced in the inner shelf flowing toward the continental slope and rise (Jacob, 2004), resulting in the poor preservation of $CaCO_3$ within the sediments.

6. Conclusions

To comprehend the changes in glaciomarine sedimentation on the continental slope and

618 continental rise of the central Ross Sea since the LGM, box and gravity cores were obtained
619 at three sites (C1, C2, and C3), on the eastern side of the Hillary Canyon. The
620 sedimentological, geochemical, and isotopic properties of core sediments were analyzed
621 along with AMS ^{14}C dating of the bulk sediments. By comparing the box cores with the top
622 of gravity cores, it was observed that the core-top loss of gravity cores is negligible, and the
623 core-top sediments efficiently preserve the Holocene record. The core-top sediments yielded
624 relatively old AMS ^{14}C ages (2.5 ka, 5.7 ka, and 1.5 ka in GC1, GC2, and GC3, respectively),
625 because of the old carbon in the seawater around the Antarctic continental margin. Based on
626 the analytical results and preliminary descriptive data, the lithologic facies were divided into
627 two units (A and B), and unit B was subdivided into two subunits (B1 and B2) related to
628 interglacial, deglacial, and glacial period. The sedimentation rates estimated by AMS ^{14}C ages
629 decreased with increasing water depth, but they were higher in the glacial period than in the
630 interglacial period.

631 Unit B2, interpreted as sedimentation during glacial period, showed relatively low $\delta^{15}N$
632 and TN, and high biogenic opal, TOC, $\delta^{13}C$, C/N ratio, and $CaCO_3$ content. The sediments of
633 unit B2 were transported from the continental shelf by melt-water under the ice sheet or distal
634 part of the debris flow in front of the grounding line of the continental shelf. Based on the
635 sedimentation rate of unit B2, the degree of sediment transport from the shelf area seems to
636 decrease with increasing water depth. Unit B1 could correspond to the sediments deposited
637 during the transition period from the glacial to the interglacial period. In this unit, biogenic
638 opal, TOC, $\delta^{13}C$, C/N ratio, and $CaCO_3$ content decreased and $\delta^{15}N$ and TN increased
639 gradually upward. Such geochemical signatures of unit B1 indicate that the effect of glacial
640 sediment supply was progressively reduced, with a gradual increase in the biogenic
641 productivity of surface water. Unit A, interpreted as the sediments deposited during the

642 interglacial period, showed relatively low biogenic opal, TOC, $\delta^{13}C$, C/N ratio, and $CaCO_3$
643 and high $\delta^{15}N$ and TN. The biogenic components of unit A were mainly supplied by the
644 biogenic productivity in surface water under seasonal sea ice conditions. The biogenic opal
645 and TOC content during the glacial period at Site C1 in the continental rise reflect the
646 seasonal sea ice conditions; however, Sites C2 and C3 were covered with permanent sea ice.

647 Similar to the continental shelf of the Antarctic continental margin, sedimentation in the
648 continental slope and rise of the central Ross Sea was largely affected by the advance and
649 retreat of the RIS. Due to the advanced RIS toward the shelf edge during the glacial period,
650 more sediments were transported from the continental shelf to the continental slope and rise
651 by melt-water under the ice sheet or debris flow at the front of the grounding line. During the
652 transition period, the effect of the ice sheet was gradually reduced by the retreat of RIS and
653 more biogenic sediments were supplied from the surface water. During the interglacial period,
654 downward settling of the biogenic particles that were generated by the enhanced biogenic
655 productivity in the surface water was the main source of biogenic components of sediments in
656 the continental slope and rise on the east of the Hillary Canyon in the central Ross Sea.

657

658 **Acknowledgements**

659 The captain, crew, and all onboard of the R/V ITALICA and technicians and
660 researchers of XXIX PNRA Expedition in 2014 are thanked for core sampling in the
661 framework of the PNRA-ROSSLOPE II Project. This study was carried out by the National
662 Research Foundation of Korea (2019K1A3A1A25000116 and 2019R1A2C1007701), KOPRI
663 project (PE21090), 2021 BK21 FOUR Program of Pusan National University, and the Italian
664 National Antarctic Research Program (PNRA) – ROSSLOPE II Project (PdR2013/AN2.01)
665 and partly co-funded by the Italian Foreign Ministry (MAECI) – STREAM Project.

References

Altabet, M.A., 1996. Nitrogen and carbon isotopic tracers of the source and transformation of particles in the deep Sea. In: Ittekkot, V., Schafer, P., Honjo, S., and Depetris, P.J. (Eds.), Particle Flux in the Ocean. John Wiley and Sons, New York, pp. 155–184.

Altabet, M.A., Francois, R., Murray, D.W., Prell, W.L., 1995. Climate-related variations in denitrification in the Arabian Sea from sediment $^{15}N/^{14}N$ ratios. Nature, 373, 506–509.

Anderson, J.B., 1975. Factors controlling $CaCO_3$ dissolution in the Weddell Sea from foraminiferal distribution patterns. Marine Geology, 19, 315–332.

Anderson, J.B., Brake, C.F., Myers, N.C., 1984 Sedimentation on the Ross Sea continental shelf, Antarctica. Marine Geology, 57, 295–333.

Anderson, J.B., Conway, H., Bart, P.J., Witus, A.E., Greenwood, S.L., McKay, R.M., Hall B.L., Ackert, R.P., Licht, K., Jakobsson, M., Stone, J.O., 2014. Ross Sea paleo-ice sheet drainage and deglacial history during and since the LGM. Quaternary Science Reviews, 100, 31–54.

Anderson, J.B., Kurtz, D.D., Domack, E.W., Balshaw, K.M., 1980. Glacial and glacial marine sediments of the Antarctic continental shelf. Journal of Geology, 88, 399–414.

Anderson, J.B., Shipp, S.S., Lowe, A.L., Wellner, J.S., Mosola, A.B. 2002. The Antarctic Ice Sheet during the Last Glacial Maximum and its subsequent retreat history: a review. Quaternary Science Reviews, 21, 49–70.

Anderson, J.B., Simkins, L.M., Bart, P.J., De Santis, L., Halberstadt, A.R.W., Olivo, E., Greenwood, S.L., 2019. Seismic and geomorphic records of Antarctic Ice Sheet evolution in the Ross Sea and controlling factors in its behaviour. In: Le Heron, D.P., Hogan, K.A., Phillips, E.R., Huuse, M., Busfield, M.E., Graham, A.G.C. (Eds.),

690 Glaciated Margins: The Sedimentary and Geophysical Archive. Geological Society,
691 London, Special Publications, vol. 475, pp. 223–240.
692 Andrews, J.T., Domack, E.W., Cunningham, W.L., Leventer, A., Licht, K.J., Jull, A.T.,
693 DeMaster, D.J., Jennings, A.E., 1999. Problems and possible solutions concerning
694 radiocarbon dating of surface marine sediments, Ross Sea, Antarctica. Quaternary
695 Research, 52, 206–216.
696 Arrigo, K.R., van Dijken, G.L., 2004. Annual changes in sea-ice, chlorophyll *a*, and primary
697 production in the Ross Sea, Antarctica. Deep-Sea Research II, 51, 117–138.
698 Arrigo, K.R., DiTullio, G.R., Dunbar, R.B., Robinson, D.H., VanWoert, M., Worthen, D.L.,
699 Lizotte, M.P., 2000. Phytoplankton taxonomic variability in nutrient utilization and
700 primary production in the Ross Sea. Journal of Geophysical Research (Oceans), 105,
701 8827–8846.
702 Barker, P.F., Barrett, P.J., Cooper, A.K., Huybrechts, P., 1999. Antarctic glacial history from
703 numerical models and continental margin sediments. Palaeogeography,
704 Palaeoclimatology, Palaeoecology, 150, 247–267.
705 Bart, P.J., Krogmeier, B.J., Bart, M.P., Tulaczyk, S., 2017. The paradox of a long grounding
706 during West Antarctic Ice Sheet retreat in Ross Sea. Scientific Reports, 7, 1–8.
707 Bonaccorsi, R., Brambati, A., Busetti, M., Fanzutti, G.P., 2000. Relationship Among X-Ray
708 Lithofacies, Magnetic Susceptibility, P-Wave Velocity and Bulk Density in Core
709 ANTA95-89C (Ross Sea, Antarctica): First Results. Terra Antarctica Reports, 4, 185–
710 198.
711 Brambati, A., Fanzutti, G.P., Finocchiaro, F., Melis, R., Frignani, M., Ravaioli, M., Setti, M.,
712 1997. Paleoenvironmental Record in Core Anta91- 30 (Drygalski Basin, Ross Sea,
713 Antarctica). In: Barker, P.F. and Cooper, A.K. (Eds.), Geology and Seismic Stratigraphy

714 of the Antarctic Margin 2. Antarctic Research Series vol. 71, American Geophysical
715 Union, pp. 137–151.
716 Caburlotto, A., Lucchi, R.G., De Santis, L., Macrì, P., Tolotti, R., 2010. Sedimentary
717 processes on the Wilkes Land continental rise reflect changes in glacial dynamic and
718 bottom water flow. International Journal of Earth Sciences, 99, 909–926.
719 Castagno, P., Capozzi, V., DiTullio, G.R., Falco, P., Fusco, G., Rintoul, S.R., Spezie, G.,
720 Budillon, G., 2019. Rebound of shelf water salinity in the Ross Sea. Nature
721 Communications, 10, 1–6.
722 Ceccaroni, L., Frank, M., Frignani, M., Langone, L., Ravaioli, M., Mangini, A., 1998. Late
723 Quaternary fluctuations of biogenic component fluxes on the continental slope of the
724 Ross Sea, Antarctica. Journal of Marine Systems, 17, 515–525.
725 Cozzi, S., Cantoni, C., 2011. Stable isotope ($\delta^{13}C$ and $\delta^{15}N$) composition of particulate
726 organic matter, nutrients and dissolved organic matter during spring ice retreat at Terra
727 Nova Bay. Antarctic Science, 23, 43–56.
728 Cunningham, W.L., Leventer, A., 1998. Diatom assemblages in surface sediments of the Ross
729 Sea: relationship to present oceanographic conditions. Antarctic Science, 10, 134–146.
730 Cunningham, W.L., Leventer, A., Andrews, J.T., Jennings, A.E., Licht, K.J., 1999. Late
731 Pleistocene-Holocene marine conditions in the Ross Sea, Antarctica: evidence from the
732 diatom record. The Holocene, 9,129–139.
733 DeConto, R.M., Pollard, D., 2016. Contribution of Antarctica to past and future sea-level rise.
734 Nature, 531, 591–597.
735 DeMaster, D.J., 1981. The supply and accumulation of silica in the marine environment.
736 Geochimica et Cosmochimica Acta, 45, 1715–1732.
737 DeNiro, M.J., Epstein, S., 1981. Influence of diet on the distribution of nitrogen isotopes in

738 animals. Geochimica et Cosmochimica Acta, 45, 341–351.
739 Domack, E.W., Jacobson, E. A., Shipp, S., Anderson, J.B., 1999. Late Pleistocene–Holocene
740 retreat of the West Antarctic Ice-Sheet system in the Ross Sea: Part 2—sedimentologic
741 and stratigraphic signature. Geological Society of America Bulletin, 111, 1517–1536.
742 Escutia, C., Eittreim, S.L., Cooper, A.K., Nelson, C.H., 1997. Cenozoic glaciomarine
743 sequences on the Wilkes Land continental rise, Antarctica. In: Ricci, C.A. (Eds.), The
744 Antarctic region: geological evolution and processes, Proceedings of the International
745 Symposium on Antarctic Earth Sciences 7, pp. 791–795.
746 Francois, R., Altabet, M.A., Burckle, L.H., 1992. Glacial to interglacial changes in surface
747 nitrate utilization in the Indian sector of the Southern Ocean as recorded by sediment
748 δ^{15}N. Paleoceanography, 7, 589–606.
749 Friedman, G.M., Sanders, J.E., 1978. Principles of Sedimentology. John Wiley and Sons.
750 New York.
751 Frignani, M., Giglio, F., Langone, L., Ravaioli, M., Mangini, A., 1998. Late Pleistocene-
752 Holocene sedimentary fluxes of organic carbon and biogenic silica in the northwestern
753 Ross Sea, Antarctica. Annals of Glaciology, 27, 697–703.
754 Gales, J., Rebesco, M., De Santis, L., Bergamasco, A., Colleoni, F., Kim, S., Accettella, D.,
755 Kovacevic, V., Liu, Y., Olivo, E., Colizza, E., Florindo-Lopez, C., Zgur, F., McKay, R.,
756 2021. Role of dense shelf water in the development of Antarctic submarine canyon
757 morphology. Geomorphology, 372, 107453.
758 Gilbert, I.M., Pudsey, C.J., Murray, J.W., 1998. A sediment record of cyclic bottom-current
759 variability from the northwest Weddell Sea. Sedimentary Geology, 115, 185–214.
760 Grobe, H., Mackensen, A., 1992. Late Quaternary climatic cycles as recorded in sediments
761 from the Antarctic continental margin. In: Kennett, J.P., Warnke, D.A. (Eds.), The

762 Antarctic Paleoenvironment: A Perpective on Global Change: Part One. Antarctic
763 Research Series vol. 56, American Geophysical Union, pp. 349–376.
764 Ha, S., Khim, B.K., Cho, H.G., Colizza, E., 2018. Origin of clay minerals of core RS14-GC2
765 in the continental slope to the east of the Pennell-Iselin Bank in the Ross Sea,
766 Antarctica. Journal of Mineralogical Society of Korea, 31, 1–12. (in Korean with
767 English abstract)
768 Hall, B.L., Henderson, G.M., Baroni, C., Kellogg, T.B., 2010. Constant Holocene Southern-
769 Ocean ^{14}C reservoir ages and ice-shelf flow rates. Earth and Planetary Science Letters,
770 296, 115–123.
771 Heaton, T. J., Köhler, P., Butzin, M., Bard, E., Reimer, R. W., Austin, W. E., Bronk, R.C.,
772 Grootes, P.M., Hughen, K.A., Kromer, B., Reimer, P.J., Adkins, J., Burke, A., Cook,
773 M.S., Olsen, J., Skinner, L.C., 2020. Marine20—the marine radiocarbon age calibration
774 curve (0–55,000 cal BP). Radiocarbon, 62, 779–820.
775 Hillenbrand, C.D., Crowhurst, S.J., Williams, M., Hodell, D.A., McCave, I.N., Ehrmann, W.,
776 Xuan, C., Piotrowski, A.M., Hernández-Molin, F.J., Graham, A.G.C., Grobe, H.,
777 Williams, T.J., Horrocks, J.R., Allen, C.S., Larter, R.D., 2021. New insights from multi-
778 proxy data from the West Antarctic continental rise: Implications for dating and
779 interpreting Late Quaternary palaeoenvironmental records. Quaternary Science
780 Reviews, 257, 106842
781 Hillenbrand, C.D., Smith, J.A., Kuhn, G., Esper, O., Gersonde, R., Larter, R.D., Maher, B.,
782 Moreton, S.G., Shimmield, T.M., Korte, M., 2010. Age assignment of a diatomaceous
783 ooze deposited in the western Amundsen Sea Embayment after the Last Glacial
784 Maximum. Journal of Quaternary Science, 25, 280–295.
785 Howat, I.M., Domack, E.W., 2003. Reconstructions of western Ross Sea palaeo- ice- stream

grounding zones from high- resolution acoustic stratigraphy. Boreas, 32, 56–75.

Jacobs, S.S., 2004. Bottom water production and its links with the thermohaline circulation. Antarctic Science, 16, 427–437.

Khim, B.K., Colizza, E., Lee, J.I., Giglio, F., Ha, S., Bak, Y.S., 2021. Biological productivity and glaciomarine sedimentation in the Central Basin of the northwestern Ross Sea since the last glacial maximum. Polar Science, 28, 100682.

Kim, S., Lee, J.I., McKay, R.M., Yoo, K.C., Bak, Y.S., Lee, M.K., Roh, Y.H., Yoon, H.I., Moon H.S., Hyun, C.U., 2020. Late Pleistocene paleoceanographic changes in the Ross Sea–Glacial-interglacial variations in paleoproductivity, nutrient utilization, and deep-water formation. Quaternary Science Reviews, 239, 106356.

Kristensen, E., Blackburn, T.H., 1987. The fate of organic carbon and nitrogen in experimental marine sediment systems: influence of bioturbation and anoxia. Journal of Marine Research, 45, 231–257.

Kuvaas, B., Leitchenkov, G., 1992. Glaciomarine turbidite and current controlled deposits in Prydz Bay, Antarctica. Marine Geology, 108, 365–381.

Langone, L., Frignani, M., Labbrozzi, L., Ravaioli, M., 1998. Present-day biosiliceous sedimentation in the northwestern Ross Sea, Antarctica. Journal of Marine Systems, 17, 459–470.

Langone, L., Frignani, M., Ravaioli, M., Bianchi, C., 2000. Particle fluxes and biogeochemical processes in an area influenced by seasonal retreat of the ice margin (northwestern Ross Sea, Antarctica). Journal of Marine Systems, 27, 221–234.

Larter, R.D., Barker, P.F., 1989. Seismic stratigraphy of the Antarctic Peninsula Pacific margin: A record of Pliocene-Pleistocene ice volume and paleoclimate. Geology, 17, 731–734.

Ledford-Hoffman, P.A., DeMaster, D.J., Nittrouer, C.A, 1986. Biogenic-silica accumulation in the Ross Sea and the importance of Antarctic continental-shelf deposits in the marine silica budget. Geochimica et Cosmochimica Acta, 50, 2099–2110.

Licht, K.J., Dunbar, N.W., Andrews, J.T., Jennings, A.E., 1999. Distinguishing subglacial till and glacial marine diamictons in the western Ross Sea, Antarctica: Implications for a last glacial maximum grounding line. Geological Society of America Bulletin, 111, 91–103.

Licht, K.J., Jennings, A.E., Andrews, J.T., Williams, K.M., 1996. Chronology of late Wisconsin ice retreat from the western Ross Sea, Antarctica. Geology, 24, 223–226.

Licht, K.J., Lederer, J.R., Swope, R.J., 2005. Provenance of LGM glacial till (sand fraction) across the Ross embayment, Antarctica. Quaternary Science Reviews, 24, 1499–1520.

Livingstone, S.J., Cofaigh, C.Ó., Stokes, C.R., Hillenbrand, C.D., Vieli, A., Jamieson, S.S., 2012. Antarctic palaeo-ice streams. Earth-Science Reviews, 111, 90–128.

Lucchi, R. G., Rebesco, M., 2007. Glacial contourites on the Antarctic Peninsula margin: insight for palaeoenvironmental and palaeoclimatic conditions. In: Viana, A.L. and Rebesco, M. (Eds.), Economic and Paleoceanographic Significance of Contourite Deposits. Geological Society of London, Special Publications, vol. 276, pp. 111–127.

Mackensen, A., 2004. Changing Southern Ocean palaeocirculation and effects on global climate. Antarctic Science, 16, 369–386.

Martin, S., 2001. Polynyas. In: Steele, J.H., Thorpe, S.A., and Turekian.K.K. (Eds.), Encyclopedia of Ocean Sciences. Academic Press, San Diego, pp. 2241–2247

McGlannan, A.J., Bart, P.J., Chow, J.M., DeCesare, M., 2017. On the influence of post-LGM ice shelf loss and grounding zone sedimentation on West Antarctic ice sheet stability. Marine Geology, 392, 151–169.

McKay, R.M., Dunbar, G.B., Naish, T.R., Barrett, P.J., Carter, L., Harper, M., 2008. Retreat history of the Ross Ice Sheet (Shelf) since the Last Glacial Maximum from deep-basin sediment cores around Ross Island. Palaeogeography, Palaeoclimatology, Palaeoecology, 260, 245–261.

Melis, R., Salvi, G., 2009. Late Quaternary foraminiferal assemblages from western Ross Sea (Antarctica) in relation to the main glacial and marine lithofacies. Marine Micropaleontology, 70, 39–53.

Meyers, P.A., 1994. Preservation of elemental and isotopic source identification of sedimentary organic matter. Chemical Geology, 114, 289–302.

Mezgec, K., Stenni, B., Crosta, X., Masson-Delmotte, V., Baroni, C., Braida, M., Ciardini, V., Colizza, E., Melis, M., Salvatore, C., Severi, M., Scarchilli, C., Traversi, R., Udisti, R., Frezzotti, M., 2017. Holocene sea ice variability driven by wind and polynya efficiency in the Ross Sea. Nature Communications, 8, 1–12.

Mollenhauer, G., Grotheer, H., Gentz, T., Bonk, E., and Hefter, J., 2021. Standard operation procedures and performance of the MICADAS radiocarbon laboratory at Alfred Wegener Institute (AWI), Germany. Nuclear Instruments and Methods in Physics Research Section B: Beam Interactions with Materials and Atoms, 496: 45–51

Mortlock, R.A., Froelich, P.N., 1989. A simple method for the rapid determination of biogenic opal in pelagic marine sediments. Deep-Sea Research A, 36, 1415–1426.

Mosola, A.B., Anderson, J.B., 2006. Expansion and rapid retreat of the West Antarctic Ice Sheet in eastern Ross Sea: possible consequence of over-extended ice streams? Quaternary Science Reviews, 25, 2177–2196.

O'Brien, P.E., Post, A.L., Edwards, S., Martin, T., Caburlotto, A., Donda, F., Leitchenkov, G., Romeo, R., Duffy, M., Evangelinos, D., Holder, L., Leventer, A., López-Quirós, A.,

858 Opdyke, B.N. Armand, L.K., 2020. Continental slope and rise geomorphology seaward
859 of the Totten Glacier, East Antarctica (112°E-122°E). Marine Geology, 427, 106221.
860 Ó Cofaigh, C., Dowdeswell, J.A., Pudsey, C.J., 2001. Late Quaternary iceberg rafting along
861 the Antarctic Peninsula continental rise and in the Weddell and Scotia Seas. Quaternary
862 Research, 56, 308–321.
863 Ogura, T.O., Abe- Ouchi, A., 2001. Influence of the Antarctic ice sheet on southern high
864 latitude climate during the Cenozoic: Albedo vs topography effect. Geophysical
865 Research Letters, 28, 587–590.
866 Pattyn, F., Ritz, C., Hanna, E., Asay-Davis, X., DeConto, R., Durand, G., Favier, L., Fettweis,
867 X., Goelzer, H., Golledge, N.R., Munneke, P.K., Lenaerts, J.T.M., Nowicki, S., Payne,
868 A.J., Robinson, A., Seroussi, H., Trusel, L.D., Van den Broeke, M., 2018. The
869 Greenland and Antarctic ice sheets under 1.5ºC global warming. Nature Climate
870 Change, 8, 1053–1061.
871 PNRA–ENEA/UTA, 2014. Rapporto sulla Campagna Antartica –Estate Australe 2013-2014 –
872 XXIX spedizione. ISSN 17232-7084, 212 pp.
873 Prothro, L.O., Majewski, W., Yokoyama, Y., Simkins, L.M., Anderson, J.B., Yamane, M.,
874 Miyairi, Y., Ohkouchi, N., 2020. Timing and pathways of east Antarctic ice sheet retreat.
875 Quaternary Science Reviews, 230, 106166.
876 Prothro, L.O., Simkins, L.M., Majewski, W., Anderson, J.B., 2018. Glacial retreat patterns
877 and processes determined from integrated sedimentology and geomorphology records.
878 Marine Geology, 395, 104–119.
879 Pudsey, C.J., 1992. Late Quaternary changes in Antarctic Bottom Water velocity inferred
880 from sediment grain size in the northern Weddell Sea. Marine Geology, 107, 9–33.
881 Pudsey, C.J., 2000. Sedimentation on the continental rise west of the Antarctic Peninsula over

the last three glacial cycles. Marine Geology, 167, 313–338.

Pudsey, C.J., Camerlenghi, A., 1998. Glacial–interglacial deposition on a sediment drift on the Pacific margin of the Antarctic Peninsula. Antarctic Science, 10, 286–308.

Pudsey, C.J., Murray, J.W., Appleby, P., Evans, J., 2006. Ice shelf history from petrographic and foraminiferal evidence, Northeast Antarctic Peninsula. Quaternary Science Reviews, 25, 2357–2379.

Rau, G.H., Froelich, P.N., Takahashi, T.D., Des Marais, D.J., 1991. Does sedimentary organic δ13C record variations in Quaternary ocean [$CO_{2(aq)}$]? Paleoceanography, 6, 335–347.

Rau, G.H., Riebesell, U., Wolf- Gladrow, D., 1997. CO_{2aq}- dependent photosynthetic ^{13}C fractionation in the ocean: A model versus measurements. Global Biogeochemical Cycles, 11, 267–278.

Reimer, P. J., Bard, E., Bayliss, A., Beck, J. W., Blackwell, P. G., Ramsey, C. B., Buck, C., Cheng, H., Edwards, L. Friedrich, M., Grootes P.M., Guilderson, T.P., Haflidason, G., Hajdas, I., Hatte, C., Heaton, T.J., Hoffmann, D.L., Hogg, A.G., Hughen, K.A., Kaiser, K.F., Kromer, B., Manning, S.W., Niu, M., Reimer, R.W., Richards, D.A., Scott, E.M., Southon, J.R., Staff, R.A., Turney, C.S.M., Van Der Plicht, J., 2013. IntCal13 and Marine13 radiocarbon age calibration curves 0–50,000 years cal BP. Radiocarbon, 55, 1869–1887.

Rignot, E., Bamber, J.L., Van Den Broeke, M.R., Davis, C., Li, Y., Van De Berg, W.J., Van Meijgaard, E., 2008. Recent Antarctic ice mass loss from radar interferometry and regional climate modelling. Nature Geoscience, 1, 106–110.

Ritz, C., Edwards, T.L., Durand, G., Payne, A.J., Peyaud, V., Hindmarsh, R.C., 2015. Potential sea-level rise from Antarctic ice-sheet instability constrained by observations. Nature, 528, 115–118.

Robinson, R.S., Sigman, D.M., 2008. Nitrogen isotopic evidence for a poleward decrease in surface nitrate within the ice age Antarctic. Quaternary Science Reviews, 27, 1076–1090.

Salvi, C., Busetti, M., Marinoni, L., Brambati, A., 2006. Late Quaternary glacial marine to marine sedimentation in the Pennell Trough (Ross Sea, Antarctica). Palaeogeography, Palaeoclimatology, Palaeoecology, 231, 199–214.

Shipp, S., Anderson, J.B., Domack, E.W., 1999. Seismic signature of the Late Pleistocene fluctuation of the West Antarctic Ice Sheet system in Ross Sea: a new perspective, Part I. Geological Society of America Bulletin, 111, 1486–1516.

Smith, J.A., Graham, A.G., Post, A.L., Hillenbrand, C.D., Bart, P.J., Powell, R.D., 2019. The marine geological imprint of Antarctic ice shelves. Nature Communications, 10, 1–16.

Smith, J.A., Hillenbrand, C.D., Pudsey, C.J., Allen, C.S., Graham, A.G., 2010. The presence of polynyas in the Weddell Sea during the Last Glacial Period with implications for the reconstruction of sea-ice limits and ice sheet history. Earth and Planetary Science Letters, 296, 287–298.

Smith Jr, W.O., Ainley, D.G., Arrigo, K.R., Dinniman, M.S., 2014. The oceanography and ecology of the Ross Sea. Annual Review of Marine Science, 6, 469–487.

Stuiver, M., Reimer, P.J., Reimer, R.W., 2018. CALIB 7.1. 2017. URL: http://calib.org (accessed: 30.11. 2017).

Tesi, T., Belt, S. T., Gariboldi, K., Muschitiello, F., Smik, L., Finocchiaro, F., Giglio, F., Colizza, E., Gazzurra, G., Giordano, P., Morigi, C., Capotondi, L., Nogarotto, A., Köseoğlu, D., Roberto, A.D., Gallerani A., Langone, L., 2020. Resolving sea ice dynamics in the north-western Ross Sea during the last 2.6 ka: From seasonal to millennial timescales. Quaternary Science Reviews, 237, 106299.

930 Tolotti, R., Salvi, C., Salvi, G., Bonci, M.C., 2013. Late Quaternary climate variability as
931 recorded by micropalaeontological diatom data and geochemical data in the western
932 Ross Sea, Antarctica. Antarctic Science, 25, 804–820.
933 Tooze, S., Halpin, J.A., Noble, T.L., Chase, Z., O'Brien, P.E., Armand, L., 2020. Scratching
934 the surface: a marine sediment provenance record from the continental slope of central
935 Wilkes Land, East Antarctica. Geochemistry, Geophysics, Geosystems, 21,
936 e2020GC009156.
937 Torricella, F., Melis, R., Malinverno, E., Fontolan, G., Bussi, M., Capotondi, L., Carlo, P.D.,
938 Roberto, A.D., Geniram, A., Kuhn, G., Khim, B.K., Morigi, C., Scateni, B., Colizza, E.,
939 2021. Environmental and Oceanographic Conditions at the Continental Margin of the
940 Central Basin, Northwestern Ross Sea (Antarctica) Since the Last Glacial Maximum.
941 Geosciences, 11, 155.
942 Villinski, J.C., Dunbar, R.B., Mucciarone, D.A., 2000. Carbon 13/Carbon 12 ratios of
943 sedimentary organic matter from the Ross Sea, Antarctica: A record of phytoplankton
944 bloom dynamics. Journal of Geophysical Research (Oceans), 105, 14163–14172.
945 Wacker, L., Fahrni, S.M., Hajdas, I., Molnar, M., Synal, H.A., Szidat, S., Zhang, Y.L., 2013.
946 A versatile gas interface for routine radiocarbon analysis with a gas ion source. Nuclear
947 Instruments and Methods in Physics Research Section B: Beam Interactions with
948 Materials and Atoms, 294, 315–319.

Figure captions

Figure 1. Map of the study area showing the location of the coring sites. Three gravity (GC1, GC2, and GC3) and box (BC1, BC2, and BC3) cores were obtained, respectively, at the three sites (RS14-C1, C2, and C3) in the continental slope and rise on the east of the Hillary Canyon in the central Ross Sea. The solid-dotted line represents the limit of advancement of the RIS during the LGM (after Anderson et al., 2019). ASC: Antarctic Slope Current, AABW: Antarctic Bottom Water, CDW: Circumpolar Deep Water, HSSW: High Salinity Shelf Water, ISW: Ice Shelf Water (Smith et al., 2014).

Figure 2. Comparison of geochemical properties (TOC, TN, and $CaCO_3$) between the box cores (BC) and the upper part of gravity cores (GC), confirming the negligible loss of core-top in the gravity core. (a) Site C1, (b) Site C2, (c) Site C3.

Figure 3. Downcore variation of sediment properties (magnetic susceptibility (MS), number of gravel-sized particles, and grain size). (a) GC3, (b) GC2, (c) GC1. Lithologic units (A, B1, and B2) are divided by solid and dotted lines and AMS ^{14}C ages are also shown.

Figure 4. XRD results for the mineral composition of IRD (bulk and ground) at 38 cm of GC3. The distinct peaks of hornblende and mica are clearly observed. Hb: hornblende, Qz: quartz, Pl: plagioclase

Figure 5. SEM-EDS results of IRDs at 38 cm of GC3. The dominant minerals are aluminosilicates including quartz. Ca peak was observed in some grains. For more results, refer to Supplementay Figure S1.

Figure 6. Downcore variation of geochemical (biogenic opal, TOC, TN, C/N, and $CaCO_3$) and isotopic ($\delta^{13}C$ and $\delta^{15}N$) properties. (a) GC3, (b) GC2, (c) GC1. Lithologic units (A, B1, and B2) are divided by solid and dotted lines and AMS ^{14}C ages are also shown.

Figure 7. Correlations between TOC and TN contents and between TOC content and C/N

ratio. (a) GC3, (b) GC2, (c) GC1.

Figure 8. Schematic model of paleoenvironmental condition showing the activity of RIS and glaciomarine sedimentation on the continental slope and rise of the central Ross Sea. (a) glacial period, (b) deglacial period, and (c) interglacial period.

List of Tables

982 Table 1. Locations of the three sites (RS14-C1, RS14-C2, and RS14-C3) in the study area.

Label	Latitude (S)	Longitude (W)	Depth (m)
RS14-C1	74°30.54’	172°51.16’	2372
RS14-C2	75°00.04’	173°55.16’	1757
RS14-C3	75°20.41’	174°36.47'	1215

983

984 Table 2. AMS ^{14}C ages of box and gravity cores.

Core	Depth (cm)	Conventional ^{14}C ages (yr BP)	Error	LCO	LCO-corrected ages (yr BP)	Calibrated ^{14}C ages (yr BP)	Laboratory code
BC1	0-1	5105	34	4005	1100	0	Poz-79258
GC1	0-1	7533	38	4006	3527	2442	Poz-69628
	4-5	11040	57	4006	7034	6701	Poz-79257
	8-9	19349	286	4006	15313	17095	AWI-4811.1.2
	26-27	29074	299	4006	25068	28040	Poz-69629
	52-53	36913	715	4006	32907	35837	Poz-69630
BC2	0-1	4275	34	3175	1100	0	Poz-79261
GC2	0-1	9320	48	3175	6142	5724	Poz-69631
	6-7	13800	67	3175	10626	10787	Poz-79266
	16-17	16660	140	3175	13484	14448	Poz-79267
	48-49	26640	243	3175	23461	26580	Poz-82577
BC3	0-1	3448	32	2348	1100	0	Poz-79268
GC3	0-1	5133	38	2348	2785	1568	Poz-69632
	12-13	6281	36	2348	3933	3287	Poz-79272
	24-25	8135	44	2348	5787	5281	Poz-82578
	50-51	26570	241	2348	24222	27210	Poz-82580

985

Figure

Click here to access/download;Figure;figures-RS14.pdf

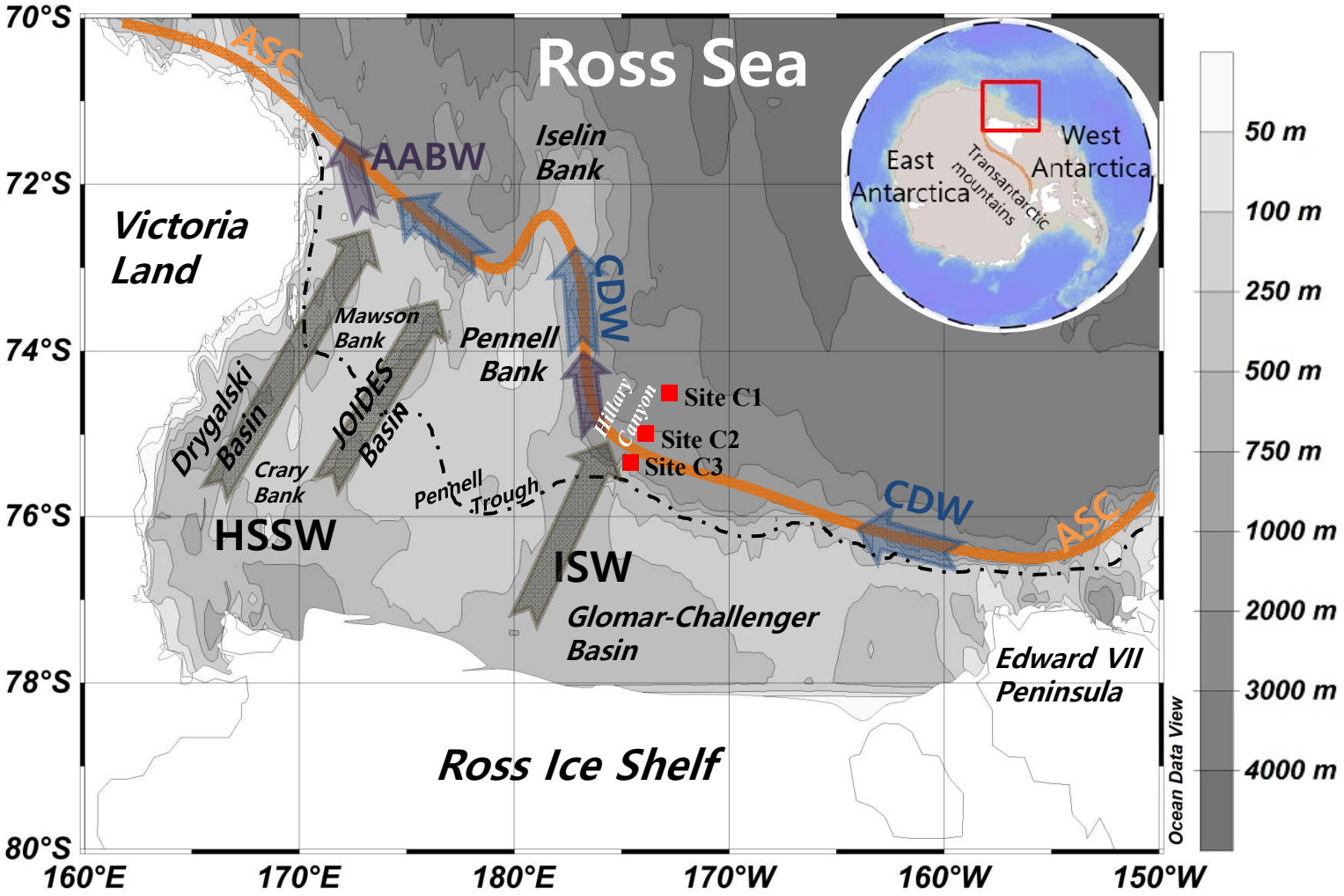

Figure 1

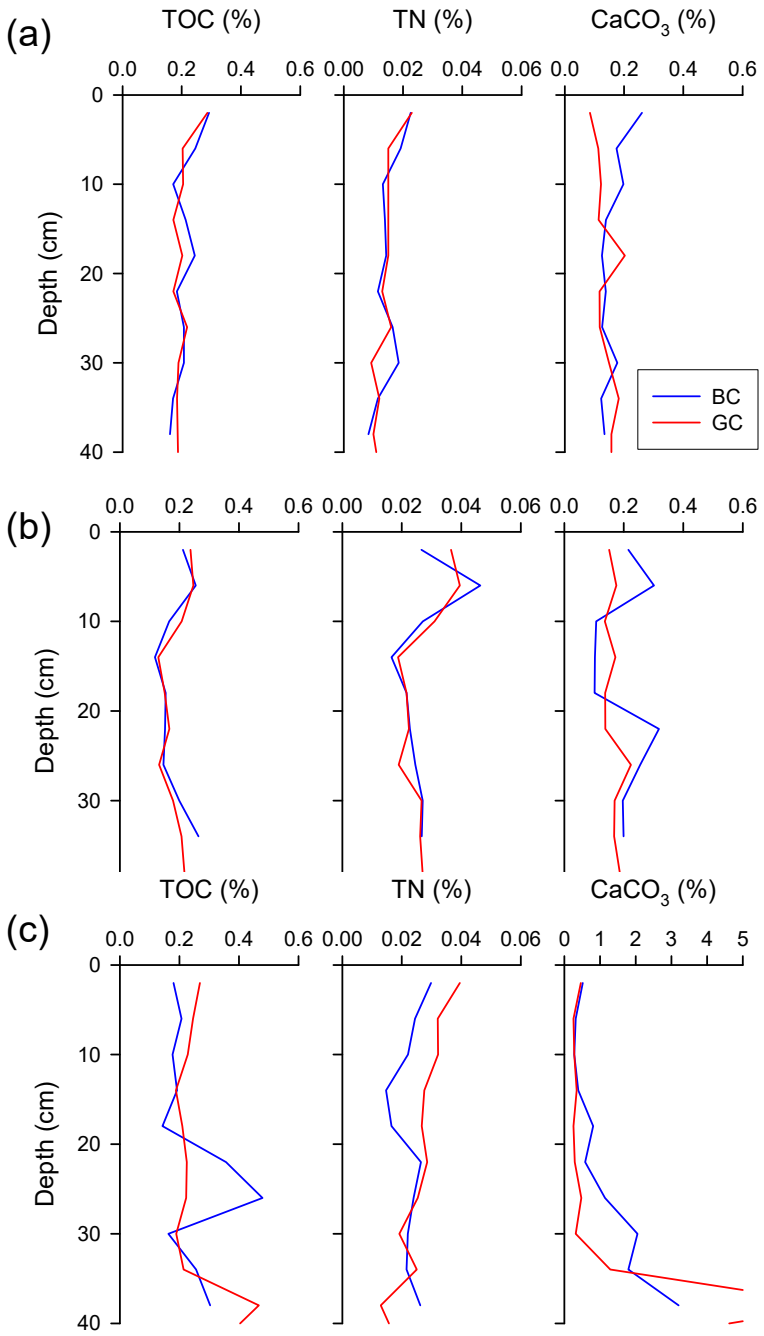
(a)
TOC (%)
TN (%)
CaCO3 (%)
0.0 0.2 0.4 0.6
0.00 0.02 0.04 0.06
0.0 0.2 0.4 0.6
Depth (cm)
0
10
20
30
40
BC
GC
(b)
0.0 0.2 0.4 0.6
0.00 0.02 0.04 0.06
0.0 0.2 0.4 0.6
Depth (cm)
0
10
20
30
TOC (%)
TN (%)
CaCO3 (%)
(c)
0.0 0.2 0.4 0.6
0.00 0.02 0.04 0.06
0 1 2 3 4 5
Depth (cm)
0
10
20
30
40

Figure 2

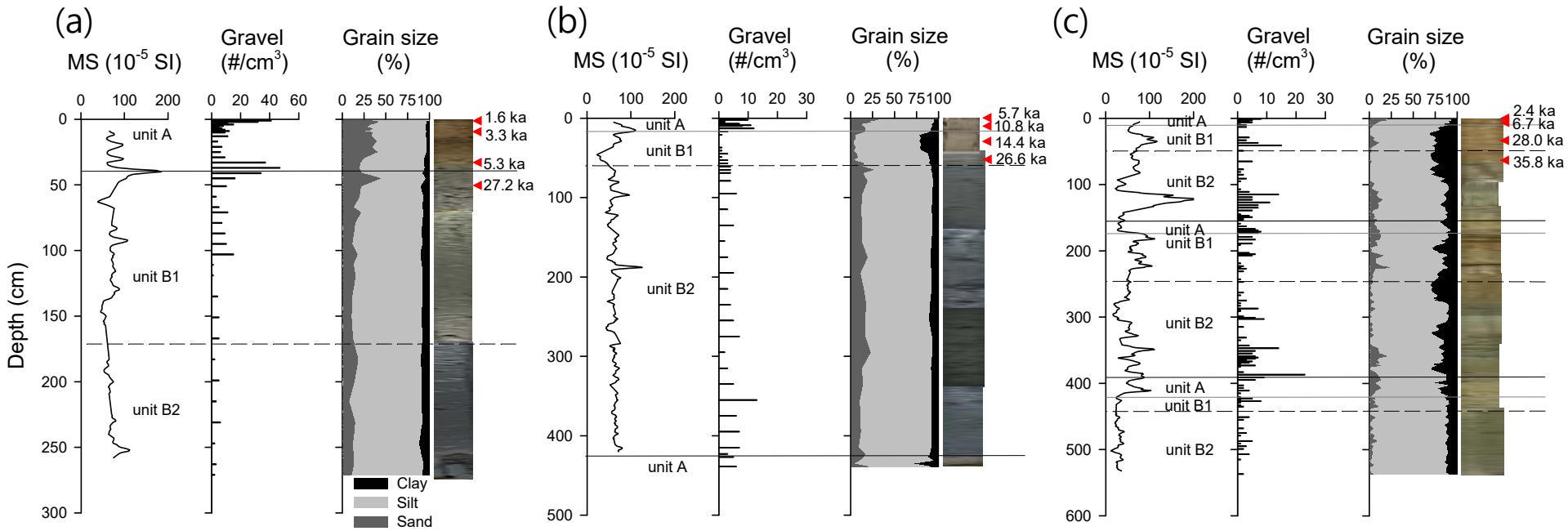
(a)
MS (10-5 SI)
Gravel (#/cm3)
Grain size (%)
Depth (cm)
unit A
unit B1
unit B2
1.6 ka
3.3 ka
5.3 ka
27.2 ka
Clay
Silt
Sand
(b)
MS (10-5 SI)
Gravel (#/cm3)
Grain size (%)
unit A
unit B1
unit B2
unit A
5.7 ka
10.8 ka
14.4 ka
26.6 ka
(c)
MS (10-5 SI)
Gravel (#/cm3)
Grain size (%)
unit A
unit B1
unit B2
unit A
unit B1
unit B2
unit A
unit B1
unit B2
2.4 ka
6.7 ka
28.0 ka
35.8 ka

Figure 3

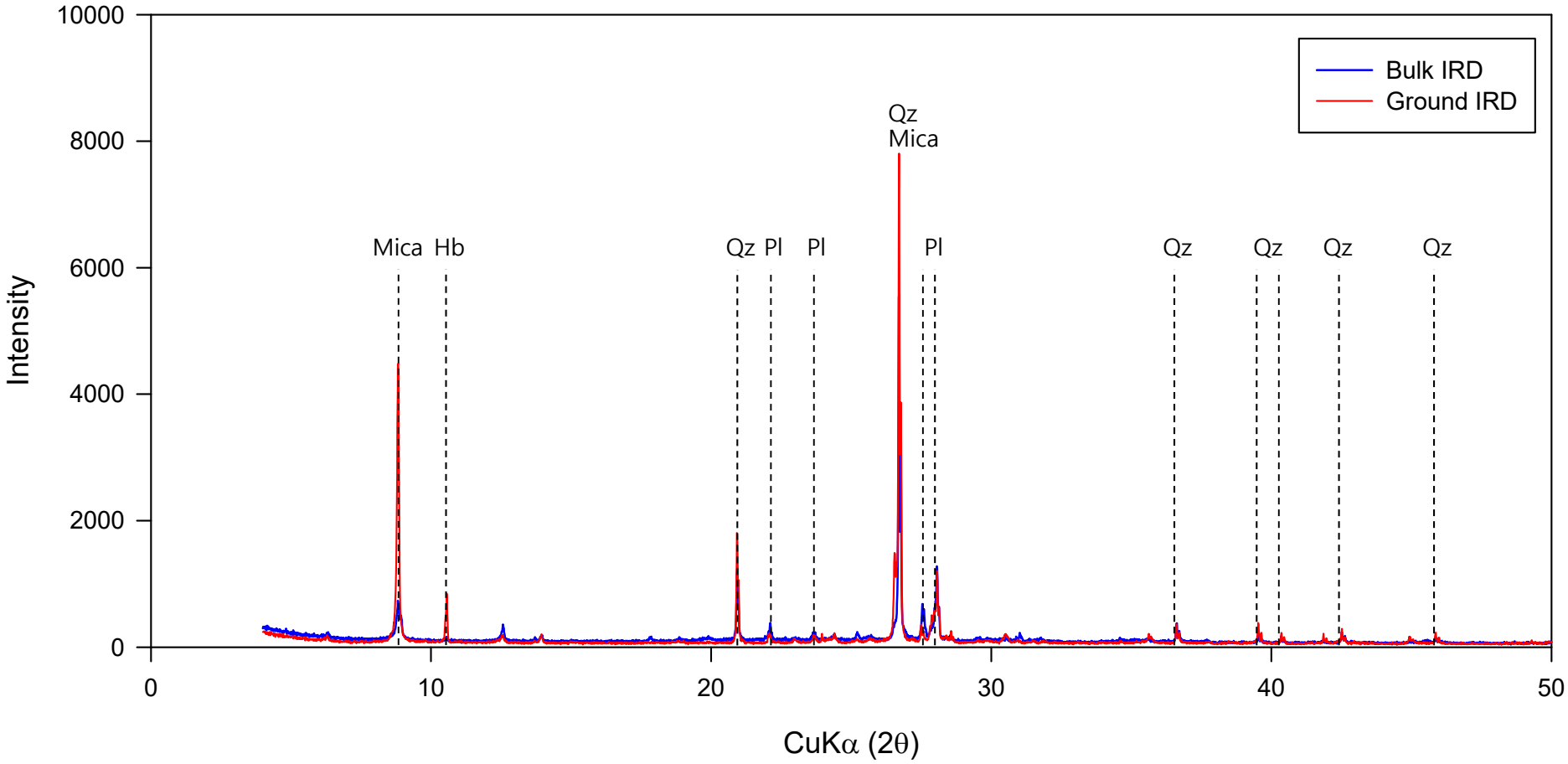
Bulk IRD
Ground IRD
Intensity
CuKα (2θ)
Mica
Hb
Qz
Pl
Pl
Qz
Mica
Pl
Qz
Qz
Qz
Qz
0
2000
4000
6000
8000
10000
0
10
20
30
40
50

Figure 4

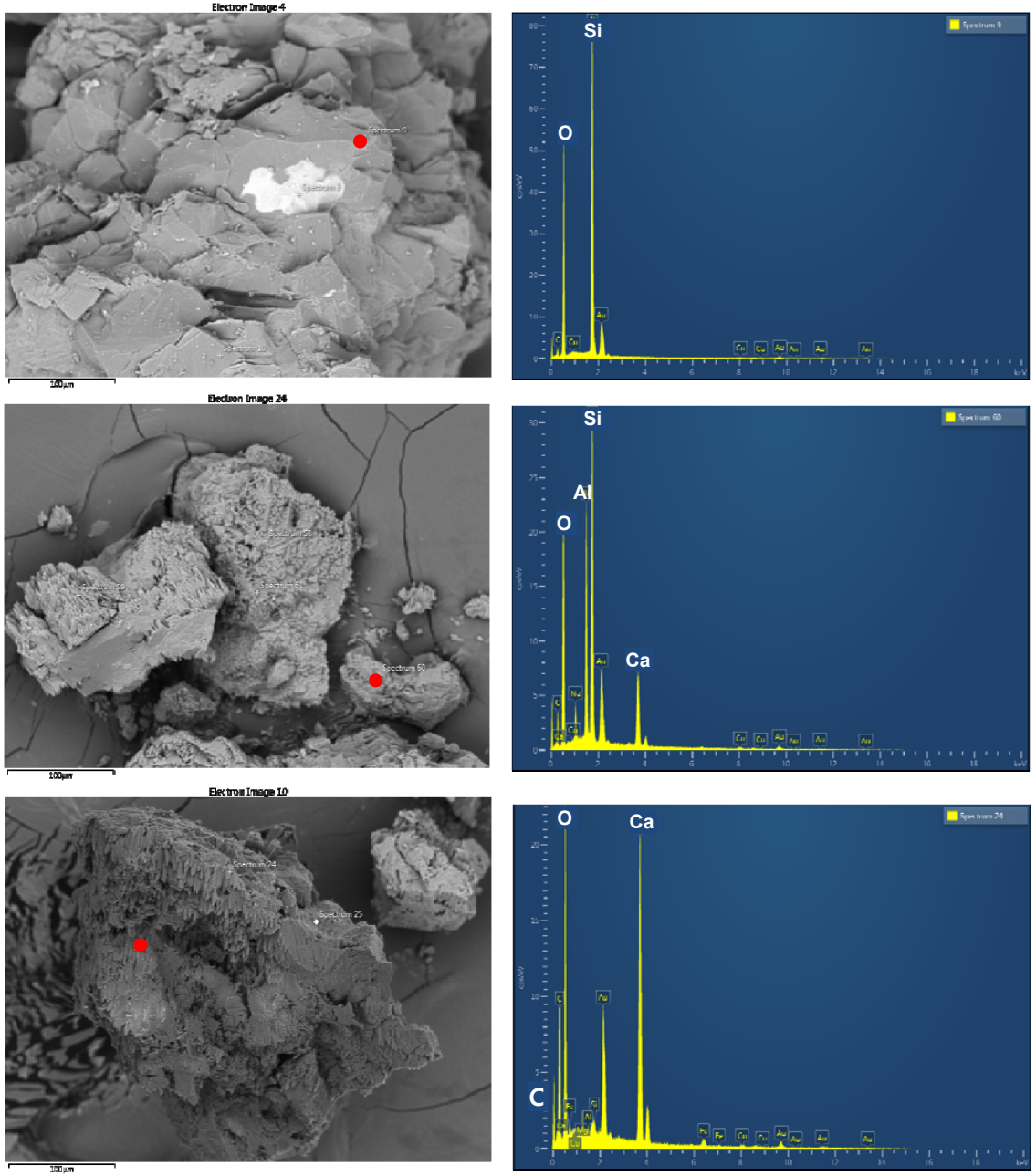
Electron Image 4
Si
O
Electron Image 24
Si
Al
O
Ca
Electron Image 10
O
Ca
C

Figure 5

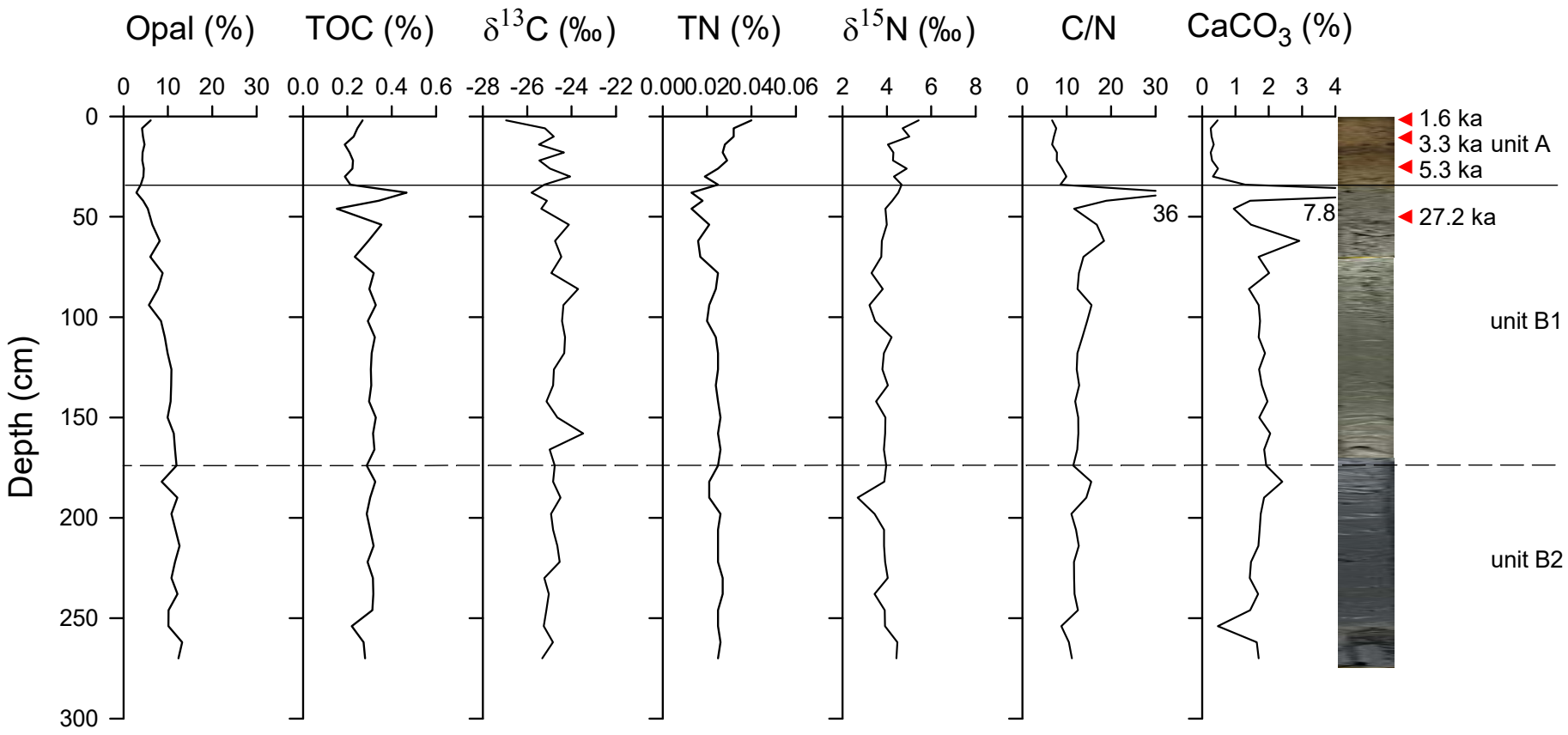
Opal (%)
TOC (%)
δ13C (‰)
TN (%)
δ15N (‰)
C/N
CaCO3 (%)
Depth (cm)
1.6 ka
3.3 ka unit A
5.3 ka
27.2 ka
unit B1
unit B2
36
7.8

Figure 6a

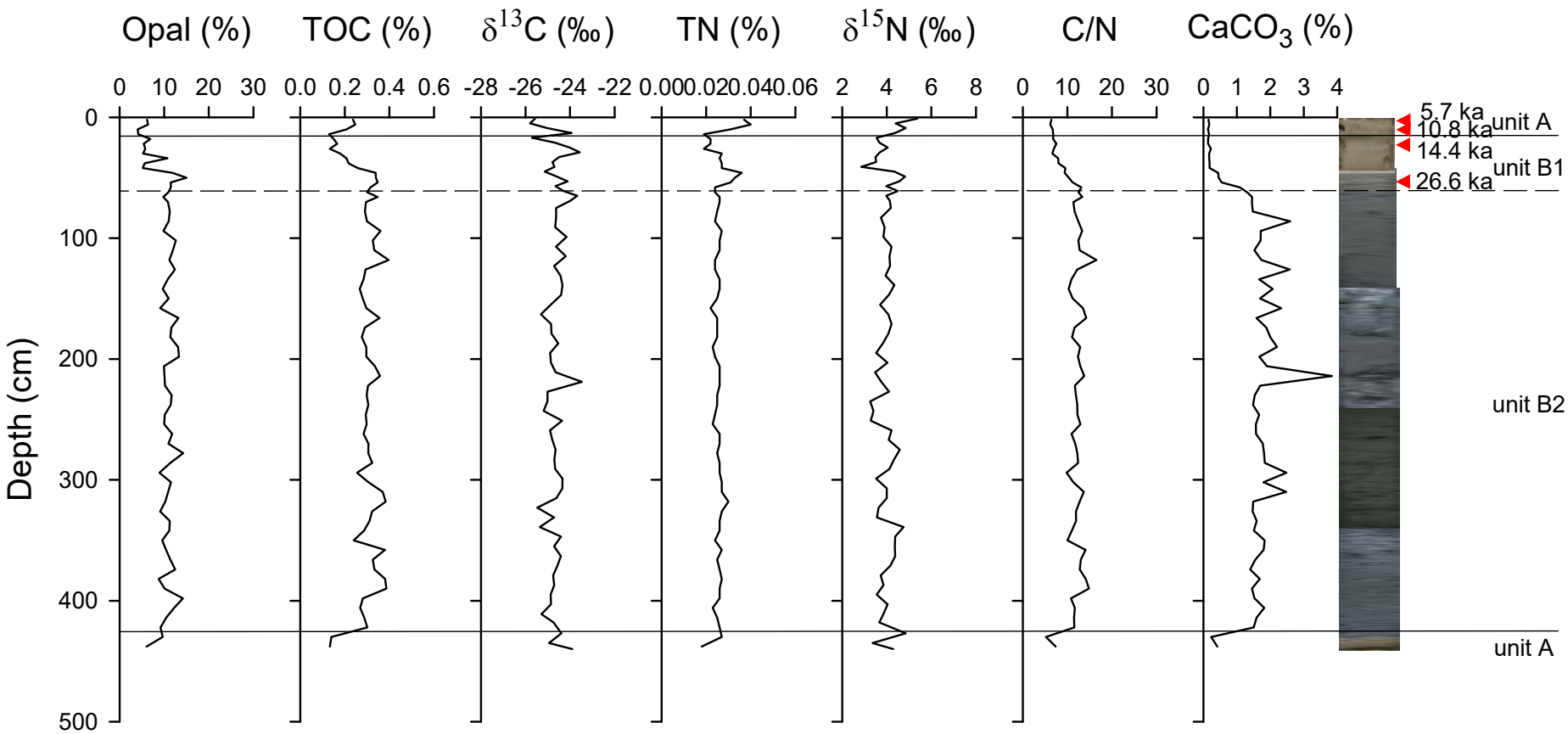
Opal (%)
TOC (%)
δ13C (‰)
TN (%)
δ15N (‰)
C/N
CaCO3 (%)
Depth (cm)
5.7 ka
10.8 ka
14.4 ka
26.6 ka
unit A
unit B1
unit B2
unit A

Figure 6b

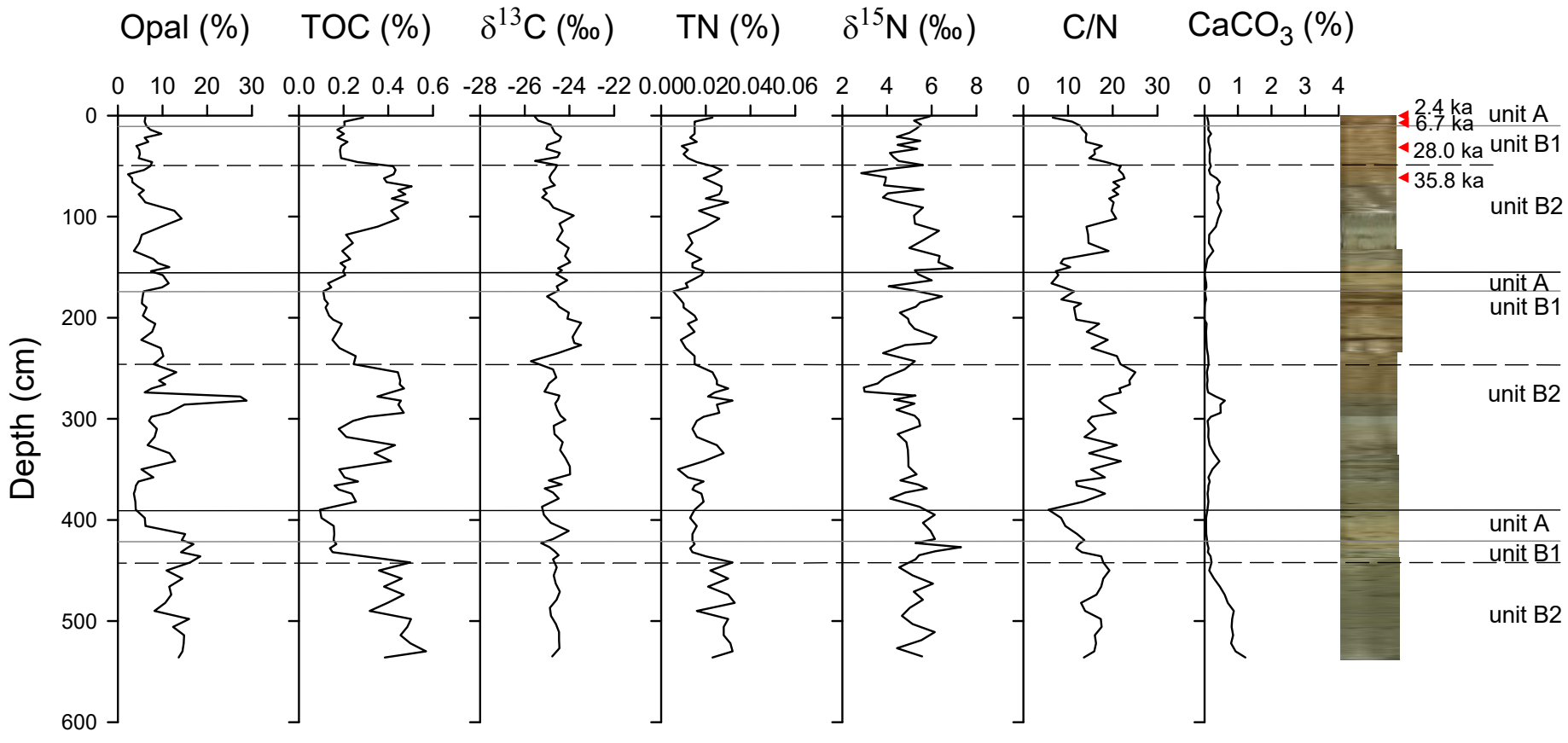
Opal (%)
TOC (%)
δ13C (‰)
TN (%)
δ15N (‰)
C/N
CaCO3 (%)
Depth (cm)
2.4 ka
6.7 ka
28.0 ka
35.8 ka
unit A
unit B1
unit B2
unit A
unit B1
unit B2
unit A
unit B1
unit B2

Figure 6c

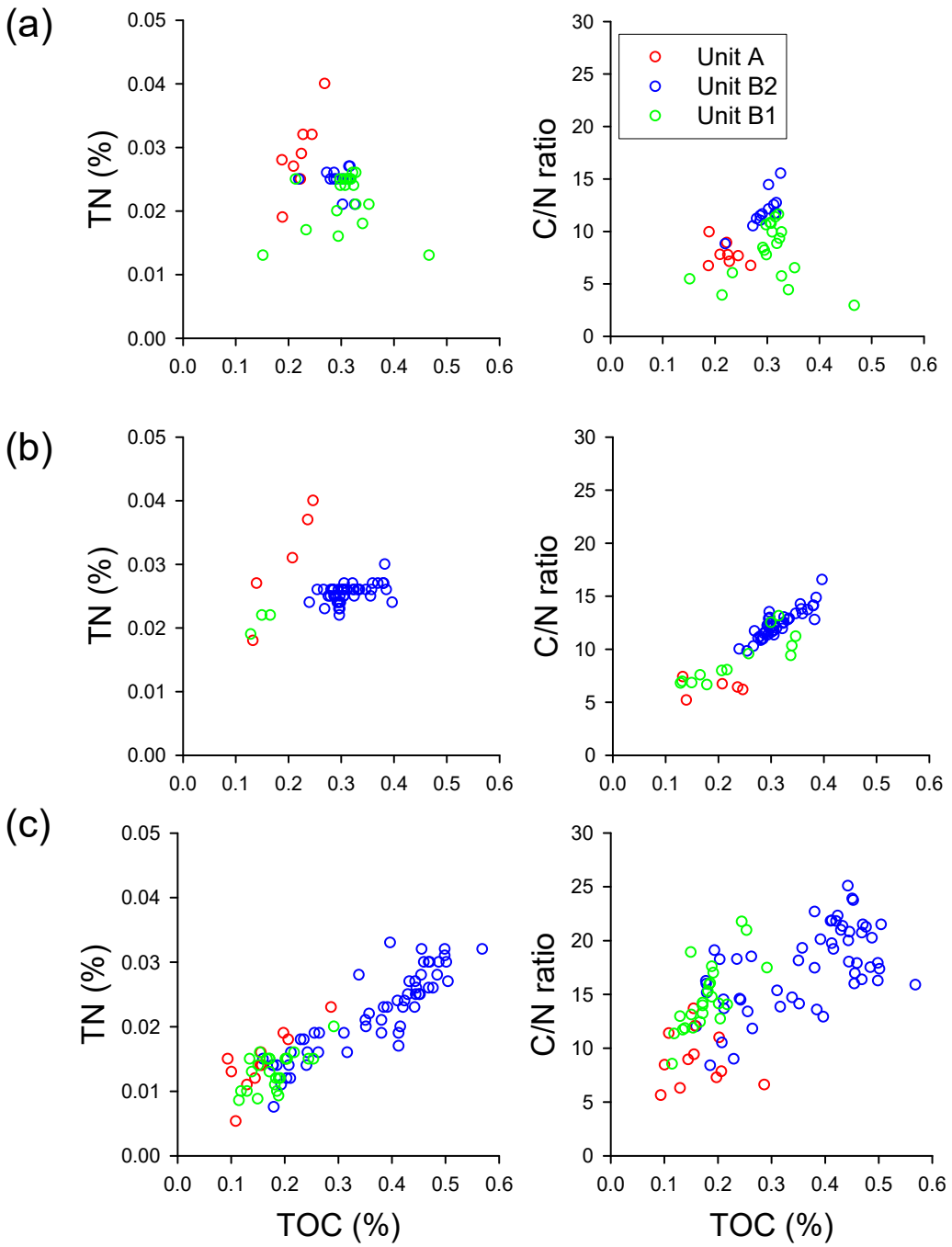
(a)
(b)
(c)
TN (%)
C/N ratio
TOC (%)
Unit A
Unit B2
Unit B1
0.00
0.01
0.02
0.03
0.04
0.05
0
5
10
15
20
25
30
0.0
0.1
0.2
0.3
0.4
0.5
0.6

Figure 7

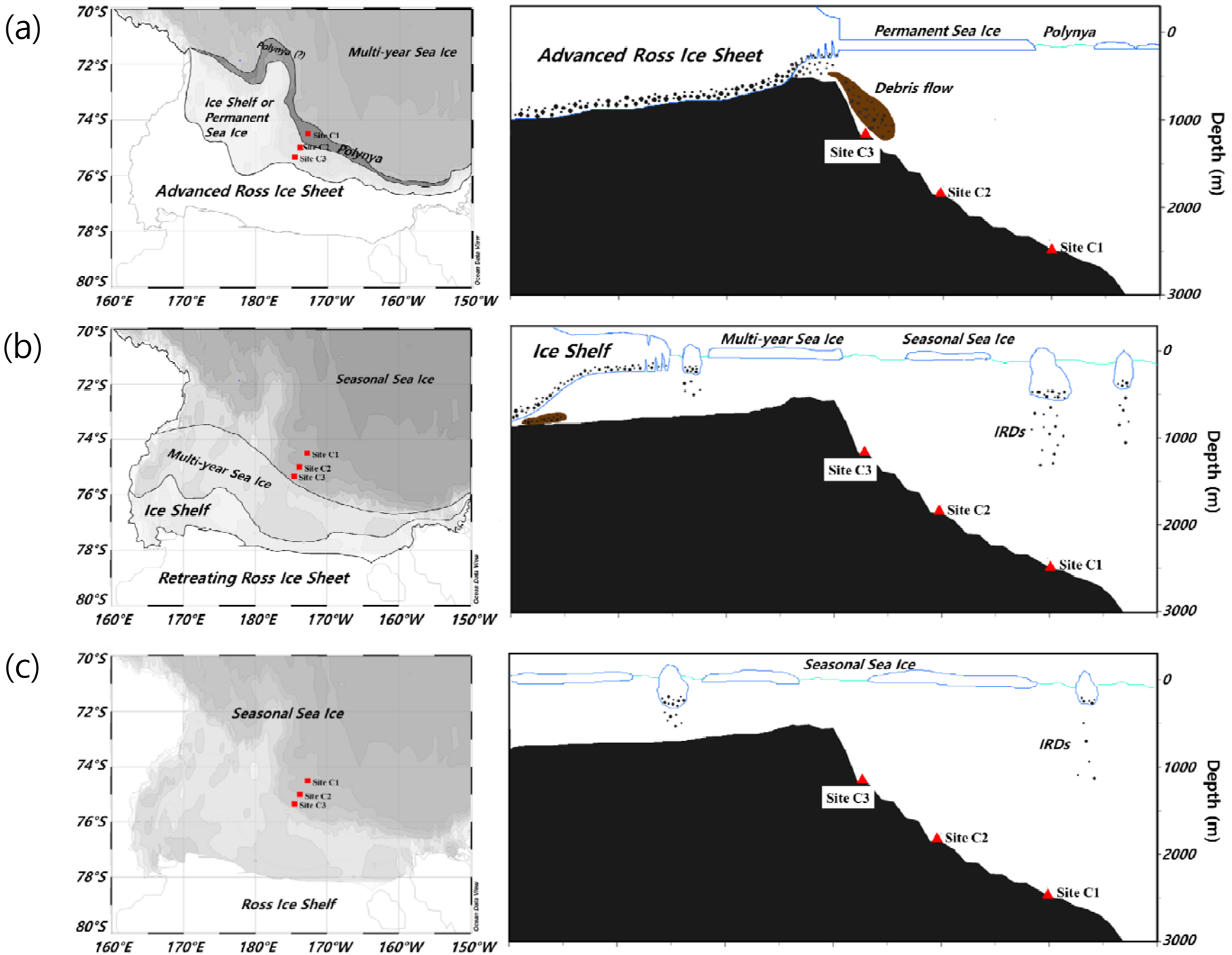
(a)
70°S
72°S
74°S
76°S
78°S
80°S
160°E
170°E
180°E
170°W
160°W
150°W
Polynya (?)
Multi-year Sea Ice
Ice Shelf or Permanent Sea Ice
Site C1
Site C2
Site C3
Polynya
Advanced Ross Ice Sheet
Advanced Ross Ice Sheet
Permanent Sea Ice
Polynya
Debris flow
Site C3
Site C2
Site C1
0
1000
2000
3000
Depth (m)
(b)
Seasonal Sea Ice
Multi-year Sea Ice
Site C1
Site C2
Site C3
Ice Shelf
Retreating Ross Ice Sheet
Ice Shelf
Multi-year Sea Ice
Seasonal Sea Ice
IRDs
Site C3
Site C2
Site C1
(c)
Seasonal Sea Ice
Site C1
Site C2
Site C3
Ross Ice Shelf
Seasonal Sea Ice
IRDs
Site C3
Site C2
Site C1

Figure 8

Declaration of interests

☒ The authors declare that they have no known competing financial interests or personal relationships that could have appeared to influence the work reported in this paper.

☐The authors declare the following financial interests/personal relationships which may be considered as potential competing interests:

Supplement Figure S1

Click here to access/download

e-Component/Supplementary data

Supplementary Data File.pdf